DOI: 10.1021/ic900914y

Inorganic Chemistry
Article

Transformations of *N*-Confused Porphyrin Triggered by Insertion of Silicon(IV)

Janusz Skonieczny, Lechosław Latos-Grażyński,* and Ludmiła Szterenberg

Department of Chemistry, University of Wrocław, F. Joliot-Curie 14, Wrocław 50-383, Poland

Received May 11, 2009

N-confused porphyrin, 5,10,15,20-tetraaryl-2-aza-21-carbaporphyrin, dissolved in triethylamine reacts with dichloromethylsilane yielding the methylsilicon(IV) complex of 5,10,15,20-tetraaryl-2-aza-21-hydroxy-21-carbaporphyrin. Addition of aldehydes or ketones (acetone, acetaldehyde acetophenone, butanone, propanal, benzaldehyde, *p*-methylbenzaldehyde, *p*-methoxybenzaldehyde, terephthaldehyde) into the insertion mixture triggered the profound transformation of *N*-confused porphyrin to form the methylsilicon(IV) complex of *N*-fused porphyrin derivative substituted at the inner C(9) position by a hydroxyalkyl moiety derived from aldehyde or ketone. The macrocyle is structurally related to an aromatic *N*-fused inner phlorin while the coordination polyhedron of bound silicon resembles the trigonal bipyramid. The macrocyclic ligand coordinates in the facial mode as the three pyrrolic nitrogen donors lie at the vertices of the single trigonal face. The meridional positions of the trigonal bipyramid are occupied by two pyrrolic nitrogen donors and a σ-methyl ligand. The coordination sphere is completed by apical coordination of the alkoxy oxygen atom derived from alkanal or alkonone. The incorporation of aldehydes and ketones is stereoselective. Acidic desililation of alkanal compounds yields two aromatic *N*-confused porphyrin derivatives, that is, 3-(1-hydroxyalkyl)-5,10,15,20-tetraaryl-2-aza-21-carbaporphyrin and its oxidation product 3-alkanoyl-5,10,15,20-tetraaryl-2-aza-21-carbaporphyrin. The acid triggered desililation of ketone derivatives produces the equimolar amounts of *N*-confused porphyrin and ketone. The first spectroscopically identified step involves the protonation of the C(7) position affording the non-aromatic silicon(IV) complex. The density functional theory (DFT) has been applied to model the molecular and electronic structure of all species identified in the course of silicon insertion into the *N*-confused and *N*-fused porphyrin.

Introduction

The coordination chemistry of *N*-confused porphyrin[1,2] has been investigated extensively over the past decade. The accumulated evidence, as recently reviewed,[3−10] has shown that *N*-confused porphyrin **1** (Chart 1) acts as suitable organometallic macrocyclic ligand toward a large variety of metal ions including transition,[11−13] main group metals[14,15] and lanthanides.[16,17] Formation of organometallic compounds which demonstrate peculiar oxidation states including the first examples of copper(II)−carbon bonds are of particular importance.[15,18−20]

While the regular porphyrin acts typically as a dianionic ligand the maximum charge of the coordinated metal ion that can be neutralized by the fully deprotonated *N*-confused porphyrin is +3. In fact *N*-confused porphyrin acts as a trianionic, dianionic, monoanionic, or as a neutral ligand with a possible involvement of all donors (internal and external) or only some of them.[4] The deprotonation level of *N*-confused porphyrin in a metal complex mainly depends on

*To whom correspondence should be addressed. E-mail: llg@wchuwr.pl.

(1) Chmielewski, P. J.; Latos-Grażyński, L.; Rachlewicz, K.; Głowiak, T. *Angew. Chem., Int. Ed. Engl.* **1994**, *33*, 779–781.
(2) Furuta, H.; Asano, T.; Ogawa, T. *J. Am. Chem. Soc.* **1994**, *116*, 767–768.
(3) Furuta, H.; Maeda, H.; Osuka, A. *Chem. Commun.* **2002**, 1795–1804.
(4) Chmielewski, P. J.; Latos-Grażyński, L. *Coord. Chem. Rev.* **2005**, *249*, 2510–2533.
(5) Latos-Grażyński, L. Core Modified Heteroanalogues of Porphyrins and Metalloporphyrins. In *The Porphyrin Handbook*; Kadish, K. M., Smith, K. M., Guilard, R., Eds.; Academic Press: New York, 2000; pp 361−416.
(6) Harvey, J. D.; Ziegler, C. J. *Coord. Chem. Rev.* **2003**, *247*, 1–19.
(7) Pawlicki, M.; Latos-Grażyński, L. *Chem. Rec.* **2006**, *6*, 64–78.
(8) Srinivasan, A.; Furuta, H. *Acc. Chem. Res.* **2005**, *38*, 10–20.
(9) Maeda, H.; Furuta, H. *Pure Appl. Chem.* **2006**, *78*, 29–44.
(10) Harvey, J. D.; Ziegler, C. J. *J. Inorg. Biochem.* **2006**, *100*, 869–880.
(11) Rachlewicz, K.; Wang, S.-L.; Ko, J.-L.; Hung, C.-H.; Latos-Grażyński, L. *J. Am. Chem. Soc.* **2004**, *126*, 4420–4431.
(12) Harvey, J. D.; Ziegler, C. J. *Chem. Commun.* **2002**, 1942–1943.
(13) Maeda, H.; Ishikawa, Y.; Matsuda, T.; Osuka, A.; Furuta, H. *J. Am. Chem. Soc.* **2003**, *125*, 11822–11823.
(14) Ogawa, T.; Furuta, H.; Takahashi, M.; Morino, A.; Uno, H. *J. Organomet. Chem.* **2000**, *611*, 551–557.
(15) Xie, Y.; Morimoto, T.; Furuta, H. *Angew. Chem., Int. Ed.* **2006**, *45*, 6907–6910.
(16) Zhu, X.; Wong, W.-K.; Lo, W.-K.; Wong, W.-Y. *Chem. Commun.* **2005**, 1022–1024.
(17) Zhu, X.; Jang, F.-L.; Poon, C.-T.; Wong, W.-K.; Wu, Y.-D. *Eur. J. Inorg. Chem.* **2008**, 3151–3162.
(18) Chmielewski, P. J.; Latos-Grażyński, L.; Schmidt, I. *Inorg. Chem.* **2000**, *39*, 5475–5482.
(19) Grzegorzek, N.; Pawlicki, M.; Szterenberg, L.; Latos-Grażyński, L. *J. Am. Chem. Soc.* **2009**, *131*, 7224−7225.
(20) Pawlicki, M.; Kańska, I.; Latos-Grażyński, L. *Inorg. Chem.* **2007**, *46*, 6575–6584.

Published on Web 07/02/2009

Chart 1. *N*-Confused **1** and *N*-Fused **2** Porphyrins

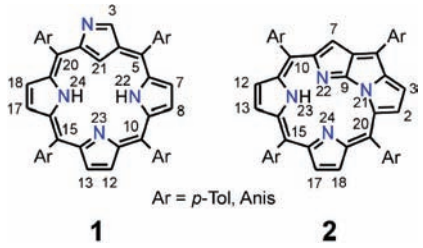

1 **2**

the metal ion charge. In general, there are three different types of coordination observed for the internal carbon of the *N*-confused pyrrole: (a) deprotonated σ-bonding carbanion of sp^2 hybridization, (b) π side-on coordination of a protonated sp^2 atom, and (c) σ-bonding of protonated sp^3 carbanion.[4,6−10]

N-confused porphyrin with its three nitrogens and one carbon donor defines the coordination site with a diameter close to 4.0 Å. Typically transition and main group cations fit easily within the *N*-confused porphyrin crevice. Alternatively the metal ion characterized by large ionic radii forms out-of-plane a complex where the metal ion resides above the *N*-confused porphyrin CN_3 plane, revealing the conformational flexibility resembling regular porphyrins.[3,5−10] Different coordination modes have been discovered once the binding of the smallest cations (boron(III) r_{cat} = 0.27 Å phosphorus(V) r_{cat} = 0.38 Å) have been explored.[21,22] The insertion of boron(III) or phosphorus(V), into the *N*-confused porphyrin triggered the *N*-confused pyrrole inversion followed by a fusion step to produce derivatives of *N*-fused porphyrin **2**.[23] Such a rearrangement can be considered as a specific mode of coordination core adjustment to given small sizes of coordinated cations.[21,22] Inversion of the *N*-confused pyrrole ring in the *N*-confused porphyrin skeleton is a prerequisite of an intramolecular fusion step which clearly demonstrates a peculiar flexibility of the [18]porphyrin (1.1.1.1)-like frame.[24,25] Actually the intermediary for fusion, that is, the inverted conformation of *N*-confused pyrrole, was trapped for the bis[iridium(I)] complex of *N*-confused porphyrin[26] or by linking of a fairly bulky group to the inner carbon.[27] Eventually a template factor can be recognized as a common driving force of fusion as the insertion of rhenium (I),[28−30] boron(III),[22] or phosphorus(V)[21] into the *N*-confused porphyrin initiated by the *N*-confused pyrrole inversion followed by a fusion step. Remarkably the coordination of phosphorus(V) or boron(III) allowed an identification of new constitutional isomers of porphyrins.[22,31] These compounds preserve the basic skeleton of maternal *N*-fused porphyrin **2**.

As a part of our systematic studies on carbaporphyrinoid(s) coordinating flexibility[4,7,32−34] we have decided to extend our recent studies devoted to insertion of boron(III) and phosphorus(V) on the silicon(IV)-*N*-confused porphyrin system. One can argue that insertion of very small elements such as silicon(IV) (r_{ion} = 0.40) may result in formation of bonds to all three nitrogen atoms and one carbon atom only if the *N*-confused porphyrin contracts significantly, which can occur through non-planar distortions of *N*-confused porphyrin similarly as determined for phosphorus(V)[35] and silicon(IV)[36−39] complexes of regular porphyrin. Till present carbaporphyrinoid chemistry of group 14 elements is limited to tin(IV) complexes of *N*-confused porphyrin and *N*-confused oxoporphyrin whereas the tin(IV) fits favorably the CN_3 coordination crevice.[15] Alternatively the insertion of silicon(IV) may initiate the macrocyclic fusion resembling the phosphorus(V) chemistry creating the contracted N_3 coordination core of *N*-fused porphyrinoids presuming that the cationic radii determine the reaction course.[21]

The present study have been focused on insertion of silicon(IV) into *N*-confused porphyrin **1**, applying dichloromethylsilane as a source of the central coordinated cation. Two types of silicon(IV) porphyrinoids have been identified. The macrocyclic ligands are structurally related to 5,10,15,20-tetraaryl-2-aza-21-carbaporphyrin (aryl: *p*-methylphenyl (*p*-Tol) or *p*-methoxyphenyl (Anis)) **1** or *N*-fused porphyrin **2**, respectively. Thus, we report the interesting case where the small cation triggers the transformation of *N*-confused porphyrin into two macrocyles of diametrically different cavity sizes and shapes. The unique incorporation of aldehydes or ketones into the hypothetical silicon(IV) *N*-fused dihydroporphyrin is of particular interest.

Results and Discussion

Insertion of Silicon(IV) to Form *N*-Confused Porphyrin Derivatives. Initial attempts to insert silicon(IV) into *N*-confused porphyrin have followed several methods developed for the preparation of (OEP)SiX_2 and (TPP)SiX_2 (OEP − dianion of 2,3,7,8,12,13,17,18-octraethylporphyrin, TPP − dianion of 5,10,15,20-tetraphenylporphyrin,

(21) Młodzianowska, A.; Latos-Grażyński, L.; Szterenberg, L. *Inorg. Chem.* **2008**, *47*, 6364–6374.
(22) Młodzianowska, A.; Latos-Grażyński, L.; Szterenberg, L.; Stępień, M. *Inorg. Chem.* **2007**, *46*, 6950–6957.
(23) Furuta, H.; Ishizuka, T.; Osuka, A.; Ogawa, T. *J. Am. Chem. Soc.* **2000**, *122*, 5748–5757.
(24) Furuta, H.; Ishizuka, T.; Osuka, A.; Ogawa, T. *J. Am. Chem. Soc.* **1999**, *121*, 2945–2946.
(25) Ishizuka, T.; Ikeda, S.; Toganoh, M.; Yoshida, I.; Ishikawa, Y.; Osuka, A.; Furuta, H. *Tetrahedron* **2008**, *64*, 4037–4050.
(26) Toganoh, M.; Konagawa, J.; Furuta, H. *Inorg. Chem.* **2006**, *45*, 3852–3854.
(27) Ishizuka, T.; Osuka, A.; Furuta, H. *Angew. Chem., Int. Ed.* **2004**, *43*, 5077–5081.
(28) Toganoh, M.; Ikeda, S.; Furuta, H. *Chem. Commun.* **2005**, 4589–4591.
(29) Toganoh, M.; Ikeda, S.; Furuta, H. *Inorg. Chem.* **2007**, *46*, 10003–10015.
(30) Toganoh, M.; Ishizuka, T.; Furuta, H. *Chem. Commun.* **2004**, 2464–2465.
(31) In this contribution to describe *N*-fused porphyrin derivatives we will use the terminology originally applied to regular porphyrin and its dihydrogenated derivatives (phlorin, isophlorin). Thus, the hypothetical macrocycle, formed by dihydrogenation of *N*-fused porphyrin **2** localized at two internal nitrogen atoms, is named *N*-fused isophlorin. Consequently the reductions involving *meso*- or inner C(9) carbon atoms will afford *N*-fused phlorin or *N*-fused inner phlorin **11**, respectively.
(32) Stępień, M.; Latos-Grażyński, L. *Acc. Chem. Res.* **2005**, *38*, 88–98.
(33) Stępień, M.; Latos-Grażyński, L.; Szterenberg, L. *Inorg. Chem.* **2004**, *43*, 6654–6662.
(34) Pacholska-Dudziak, E.; Skonieczny, J.; Pawlicki, M.; Szterenberg, L.; Ciunik, Z.; Latos-Grażyński, L. *J. Am. Chem. Soc.* **2008**, *130*, 6182–6195.
(35) Sanders, J. K. M.; Bampos, N.; Clyde-Watson, Z.; Darling, S. L.; Hawley, J. C.; Kim, H.-J.; Mak, C. C.; Webb, S. J. Axial Coordination Chemistry of Metalloporphyrins. In *The Porphyrin Handbook*; Kadish, K. M., Smith, K. M., Guilard, R., Eds.; Academic Press: San Diego, CA, 2000; pp 1−48.
(36) Kane, K. M.; Lemke, F. R. *Inorg. Chem.* **1995**, *34*, 4085–4091.
(37) Cissell, J.; Porter, W. W. III; Vaid, T. P. *J. Am. Chem. Soc.* **2005**, *127*, 12212–12213.
(38) Kane, K. M.; Lorenz, C. R.; Heilman, D. M.; Lemke, F. R. *Inorg. Chem.* **1998**, *37*, 669–673.
(39) Kane, K. M.; Lemke, F. R. *Inorg. Chem.* **1997**, *36*, 1354–1359.

Scheme 1. Synthesis of **3**-Me

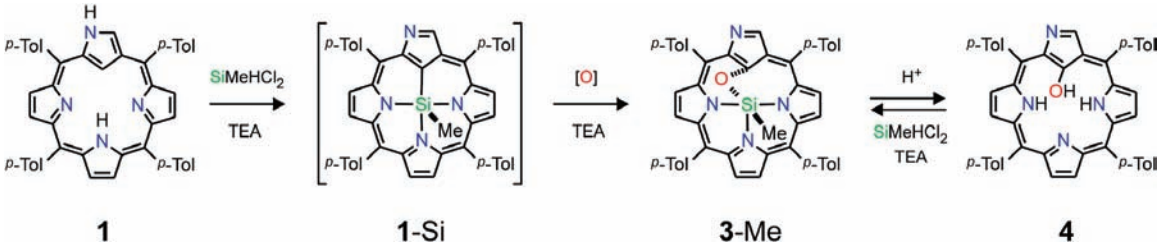

X = Cl, F, TfO). The subsequent conditions, applied previously in the literature have been originally probed in the course of our investigations. Thus the reactions of *N*-confused porphyrin with $SiCl_4$ in pyridine,[40] $SiHCl_3$ in THF,[36] or porphyrin dianion and $SiHCl_3$ in dichloromethane[38] have not resulted in the expected macrocyclic complexes containing coordinated silicon(IV) cation. Eventually we have considered several silanes ($SiMe_2Cl_2$, $SiPh_2Cl_2$, $SiMeCl_3$, $SiMeHCl_2$) as a suitable source of silicon(IV). The systematic studies demonstrated that the insertion has taken place in a single case of $SiMeHCl_2$ pointing out that the presence of the stabilizing methyl group accompanied by more reactive hydride and two chloro substituents is of importance. The similar procedure using a homologue of $SiMeHCl_2$, that is, $SiEtHCl_2$ afforded essentially similar chemistry as that observed for $SiMeHCl_2$ confirming the thesis that such specific selection of silane substituents is important. Significantly $SiMeCl_3$ fails as a silicon(IV) source (eventually *N*-confused porphyrin has been recovered) in identical reaction conditions as applied for $SiMeHCl_2$ or $SiEtHCl_2$ indicating the importance of the hydride in the process.

The synthetic procedure has been presented in Scheme 1. An addition of $SiMeHCl_2$ in excess to *N*-confused porphyrin **1** dissolved in dichloromethane resulted in the solution color change from brown-green to yellow-brown. Subsequently the pyridine or triethylamine (TEA) have been added in the 6-fold volume excess providing the appropriate solvent for the process. The use of pyridine of TEA is essential as these solvents neutralize acids released because of the insertion. Eventually silicon(IV) macrocyclic products are protected from the feasible acid accelerated desililation. In this respect, the procedure followed one described for coordination of tin(IV) by *N*-confused porphyrin.[15]

Thus *N*-confused porphyrin **1** reacts with $SiMeHCl_2$ in triethylamine (pyridine) yielding after chromatographic workup the methylsilicon(IV) complex of 5,10,15,20-tetraaryl-2-aza-21-hydroxy-21-carbaporphyrin **3**-Me. A similar coordination mode was previously determined for iron(III) complexes of 5,10,15,20-tetraaryl-2-aza-21-hydroxy-21-carbaporphyrin.[11,41] The modified macrocycle acts as a triaanionic tetradentate ligand fitting perfectly to the cationic charge of methylsilicon(IV). Thus the insertion of silicon(IV) enables the pyrrololate moiety coordination via deprotonated 21-oxygen atom. Presumably the dioxygen activation allowed insertion of oxygen atom into the silicon−carbon bond of the supposed regular methylsilicon(IV) *N*-confused porphyrin **1**-Si similarly as seen for iron(III) *N*-confused porphyrins.[11] Actually 5,10,15,20-tetraaryl-2-aza-21-hydroxy-21-carbaporphyrin **4** has been isolated via desililation of **3**-Me in acidic conditions. The isolated macrocycle reveals the similar spectroscopic features as previously reported for **4**.[42] In fact we have obtained **4** on the way of the demetalation procedure reported for iron(III) 5,10,15,20-tetraaryl-2-aza-21-hydroxy-21-carbaporphyrin.[42] The reaction of **4**, prepared by such an independent route, with $SiMeHCl_2$ readily afforded **3**-Me confirming the identity of the macrocycle.

Scheme 2. Synthesis of **6**

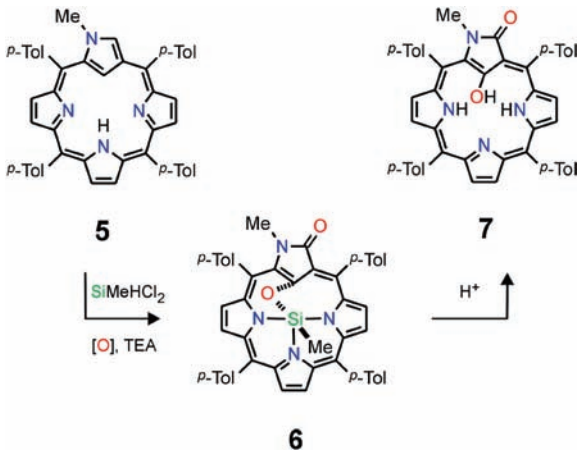

Eventually the *N*-confused porphyrin methylated at the external nitrogen atom (2-methyl-5,10,15,20-tetraaryl-2-aza-21-hydroxy-21-carbaporphyrin) **5** has been considered as an alternative ligand for formation of the silicon(IV) carbaporphyrinoid compounds (Scheme 2). The reaction of **5** with $SiMeHCl_2$ in TEA yielded **6** because of the methylsilicon(IV) coordination to 2-methyl-3-oxo-5,10,15,20-tetraaryl-2-aza-21-hydroxy-21-carbaporphyrin **7**.

The acidic desililation of **6** afforded **7** quantitatively. Thus the insertion process has been accompanied by conversion of *N*-methylated *N*-confused porphyrin **5** into 21-hydroxy-*N*-methylated derivative **7** of known *N*-confused oxoporphyrin.[15,43]

NMR Investigations. The identities of silicon(IV) porphyrinoids **3**-Me, **6**, and the free base **7** have been confirmed by high-resolution mass spectrometry and NMR

(40) Gouterman, M. Optical Spectra and Electronic Structure of Porphyrins and Related Rings. In *The Porphyrins*; Dolphin, D., Ed.; Academic Press: New York, 1978; pp 1−165.

(41) Hung, C.-H.; Chen, W.-C.; Lee, G.-H.; Peng, S.-M. *Chem.Commun.* **2002**, 1516–1517.

(42) Hung, C.-H.; Wang, S.-L.; Ko, J.-L.; Peng, C.-H.; Hu, C.-H.; Lee, M.-T. *Org. Lett.* **2004**, *6*, 1393–1396.

(43) Schmidt, I.; Chmielewski, P. J. *Tetrahedron Lett.* **2001**, *42*, 6389–6392.

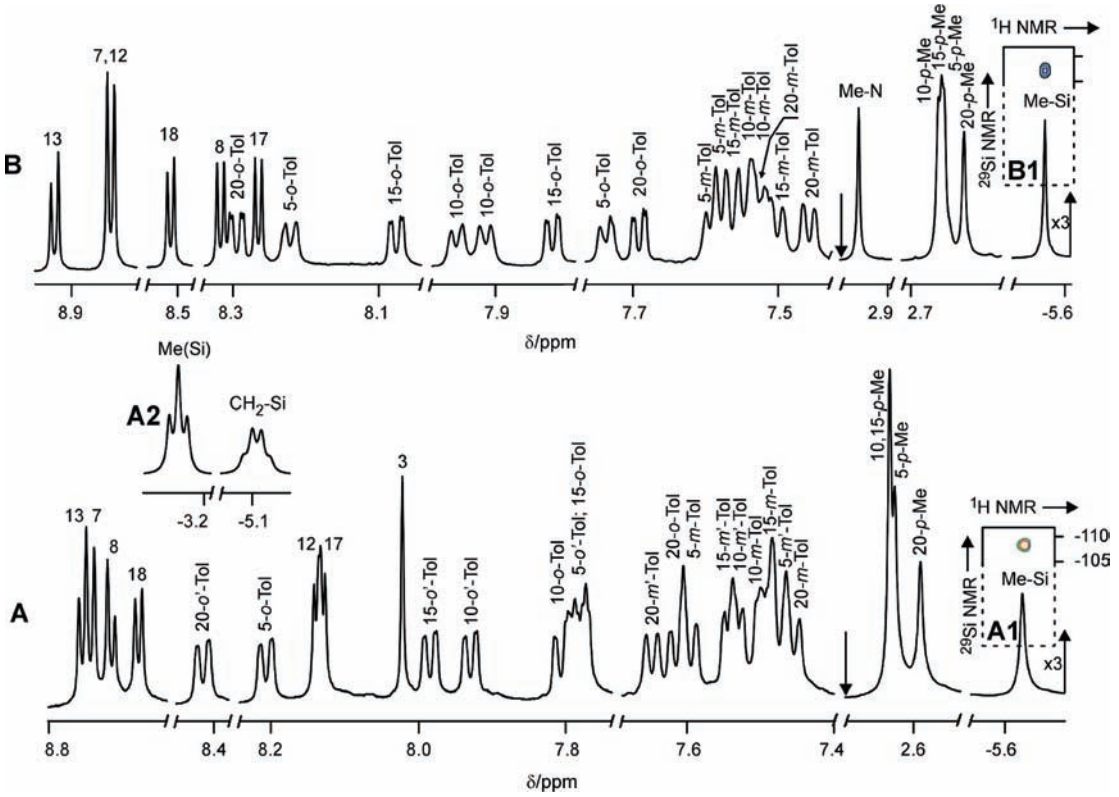

Figure 1. ^{1}H NMR spectra of (A) **3**-Me (chloroform-*d*, 230 K) and (B) **6** (chloroform-*d*, 250 K). Insets A1 and B1 show ^{1}H−^{29}Si NMR correlations (chloroform-*d*, 298 K). Inset A2 presents ^{1}H NMR spectrum (chloroform-*d*, 220 K) of **3**-Et (only signals of the Et-Si fragment are shown).

spectroscopy. Thus, the assignments of resonances, which are given above the selected groups of peaks (Figure 1) have been made on the basis of relative intensities and detailed two-dimensional NMR studies (COSY, NOESY, ^{1}H−^{13}C (HMQC, HMBC) and ^{1}H−^{29}Si (HMBC)) carried out in chloroform-*d* at temperatures adjusted to obtain the best resolution.

The straightforward allocation of SiMe resonance resulted from its remarkable upfield position because of the efficient ring current effect and has been confirmed via the ^{1}H−^{29}Si NMR scalar coupling (Figure 1, Insets A1, B1). The ^{1}H NMR spectrum of **3**-Me (230 K) exhibits three AB spin systems and a singlet assigned to the pyrrolic hydrogens. Four different sets of *meso*-*p*-tolyl ring resonances have been also detected. All of them demonstrated two ortho and two meta multiplets readily correlated via COSY and NOESY with particular methyl resonances. The detected differentiation of ortho and meta resonances seen for *p*-tolyls suggests that their rotation with respect to the C_{meso}−C_{ipso} bond is slow below 230 K reflecting the distinguishable macrocyclic sides due to the axial coordination. The structural formulas of **3**-Me and **6** shown in Schemes 2 and 3 demonstrated merely the projection facilitating a presentation. To account for the ^{1}H NMR characteristics of **3**-Me and **6** non-planar structural scaffolds have been considered.

Consequently density functional theory (DFT) studies have been used to visualize the suggested structures of silicon porphyrinoids **3**-Me (Figure 2). Geometries of **3**-Me and all other structures below were optimized at the B3LYP/6-31G** level of theory. All DFT optimization have been carried out for compounds with *p*-tolyl

Scheme 3. Acetone Addition

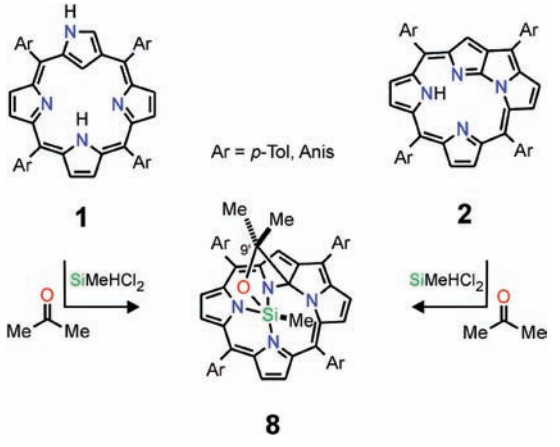

substituents at the *meso* positions. The introduction of the oxygen atom into the coordination core as shown in **3**-Me causes the macrocyclic strain, which is partly relieved by bending the pyrrolic moiety out of the N_3 macrocyclic plane as seen in Figure 2. The methyl ligand can be coordinated on one of the two inequivalent faces of the macrocycle, leading to two distinct species *syn* and *anti*. The DFT calculations demonstrated that the *anti* conformer is substantially more stable as reflected by the energy difference between $\mathbf{3}_{anti}$ and $\mathbf{3}_{syn}$ which equals 11.2 kcal/mol. Consequently the $\mathbf{3}_{anti}$ structure has been tentatively assigned to the dominating set of resonances. In fact the *anti* conformation was observed in the iron(III) complexes of **4**,[11,41] where the oxygen was inserted between

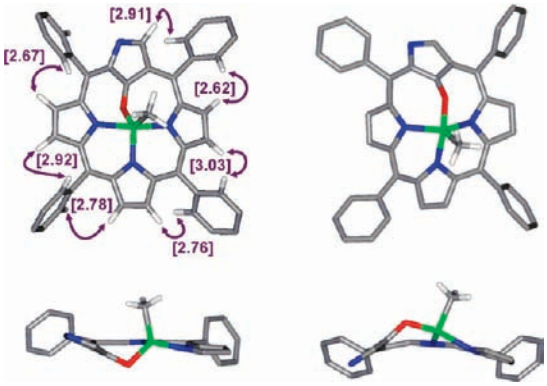

Figure 2. DFT optimized structure of $\mathbf{3}_{anti}$ (left) and $\mathbf{3}_{syn}$ (right) (up: perspective views; down: side views with *p*-Me groups removed for clarity). Only the analytically useful hydrogens are shown. The established NOE connectivities between appropriate hydrogens for $\mathbf{3}_{syn}$ are shown. The spatial proximities (in Å) are in parentheses.

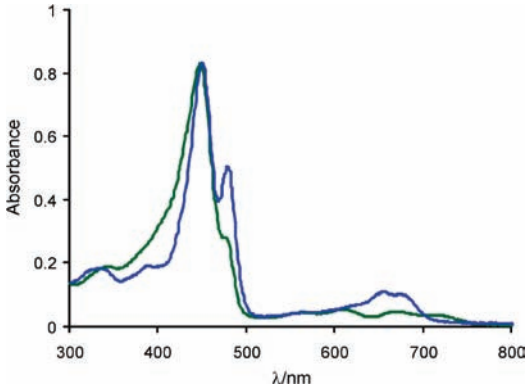

Figure 3. UV−vis spectra of **3**-Me (green) and **6** (blue) in CH_2Cl_2.

the iron(III) ion and the inner carbon atom. The optimized structure of $\mathbf{3}_{anti}$ highlights that the methyl group is located above the N_3 plane. The coordination silicon polyhedron resembles the trigonal bipyramid with the main axis determined by N(22) and N(24) nitrogen atoms whereas the O(21), N(23), and carbon atom of the methyl group occupy the meridional positions.

The straightforward assignment of H(3) resonance provided the initial step for the ^{1}H NMR analysis. Once assigned this particular resonance has been used as a starting point of NOE studies. The fundamental relays NOE connectivities are shown in Figure 2. The similar analysis have been carried for **6** using the characteristic (N)Me resonance as a starting point. Actually structural constraints determined by NOE have been built in the DFT optimized structures.

The electronic spectra of **3**-Me and **6** are shown in Figure 3. Significantly one can detect the intense bands in the region typically assigned to the Soret-like band of aromatic carbaporphyrinoids. Its high extinction coefficients, about $\log \varepsilon = 6$, imply the aromatic character of the ligand in **3**-Me and **6**.

Identification of Acetone and Acetaldehyde *N*-Fused Porphyrin Derivatives. Several attempts have been made to force the insertion of silicon(IV) into the *N*-confused porphyrin affording, as discussed above, **3**-Me and **6**, however, in rather limited yield. Our studies aimed to adjust reaction conditions have involved also the tedious analysis of all macrocyclic products. Thus, the starting *N*-confused porphyrin **1**, *N*-fused porphyrin **2**, and the *N*-confused porphyrin dimer[44] have been readily recognized and eventually separated by a column chromatography in noticeable amounts. Actually as described in the introduction the templating effect of small cations, which facilitates the conversion of *N*-confused porphyrin **1** into *N*-fused porphyrin **2** has been documented in case of boron(III) and phosphorus(V).[21,22] Here a similar role could be reasonably assigned to silicon(IV).

In addition to known compounds, the other aromatic macrocyclic derivatives with coordinated silicon(IV) have been identified. The ^{1}H NMR spectra recorded for the products of different synthesis conditions have shown three (synthesis in pyridine) or two (synthesis in TEA) upfield located methyl resonances (the −1 ppm to −4 ppm region, Figure 4) eventually assigned to the macrocyclic species **8** and **9**-**1**, respectively (Scheme 3 and 4). The molecular structures of **8** and **9**-**1** allow the simultaneous location of these methyl substituents in the diatropic deshielding zone. The crucial methyl resonances have been accompanied by an appropriate set of macrocyclic resonances situated in the region which is typical for aromatic porphyrinoids.

Once $SiMeHCl_2$ has been replaced by $SiEtHCl_2$ the reaction in pyridine led to the ethyl analogue of **3**-Me, that is, **3**-Et. The ethyl coordination has been reflected by the distinct ^{1}H NMR pattern of the upfield shifted ethyl multiplets which replace the methyl signal of Me-Si (see Inset A2 of Figure 1). The diastereotopic splitting of the methylene multiplet has been detected because of chirality of **3**-Et. As observed for **3**-Me, the synthesis of **3**-Et has been accompanied by formation of *N*-fused porphyrin. Significantly the ethyl analogue of **8**, that is, **8**-Et (Supporting Information, Figure S1) preserved two upfield methyl resonances of **8** replacing the third one by a set of ethyl multiplets as already seen for the **3**-Me−**3**-Et couple. The desililation of **8** or **8**-Et carried out by addition of $HCl_{(g)}$ or by boiling in toluene produced the *N*-fused porphyrin **2** as a single macrocyclic product. At this stage one could conclude that the peculiar transformations, although induced by silane, may require some unintentionally added components contained or formed in applied solvents.

A combination of mass spectrometry and ^{1}H NMR spectroscopy of **8** has allowed identifying acetone as a crucial substrate in the sequence of discovered transformations. Once the appropriate amount of acetone has been purposely included into a general insertion procedure the formation of **8** was systematically detected in yields comparable to **3**-Me. Significantly the replacement of regular acetone by acetone-d_6 produces the selectively deuterium labeled species **8**-d_6 as indicated by the disappearance of two methyl resonances (−1.65 and −1.84 ppm) in the ^{1}H NMR spectrum and the rise of their counterparts in the ^{2}H NMR spectrum. The straightforward comparison of the mass spectra obtained for **8** (*meso*-tetra(*p*-tolyl)) (m/z = 769.3) and **8**-d_6 (m/z = 775.4) confirms the extent of isotopic substitution consistent with the addition of the acetone moiety. In the similar approach as described for **8** the formation of **9**-**1** (Scheme 4)

(44) Chmielewski, J. P. *Angew. Chem., Int. Ed.* **2004**, *43*, 5655–5658.

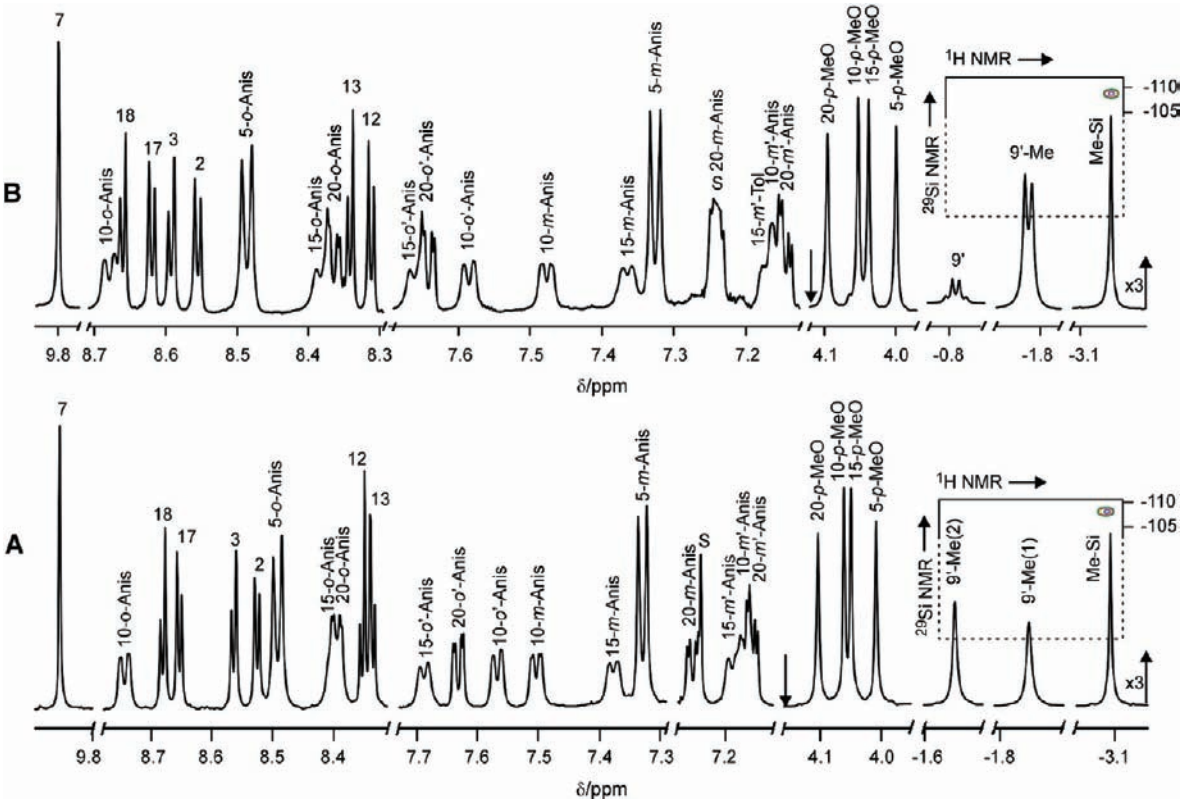

Figure 4. ^{1}H NMR spectra of (A) **8** and (B) **9-1** (chloroform-*d*, 210 K). Insets present ^{1}H−^{29}Si NMR correlations (chloroform-*d*, 298 K).

Scheme 4. Addition of Aldehydes and Ketones[a]

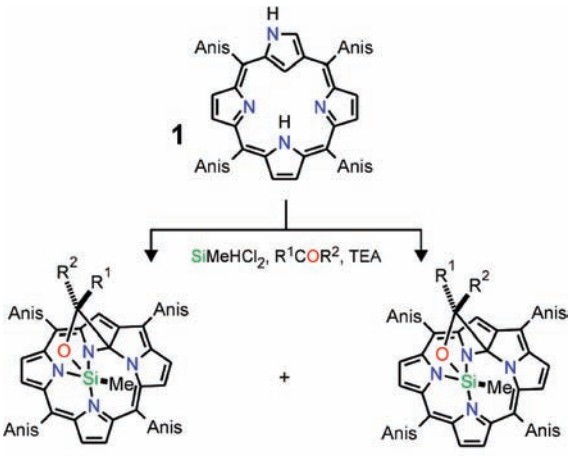

[a] **8** (R_1 = Me, R_2 = Me), **9-1** (R_1 = Me, R_2 = H), **9-2** (R_1 = Me, R_2 = H), **12-1** (R_1 = Et, R_2 = H), **12-2** (R_1 = Et, R_2 = H), **13-1** (R_1 = Et, R_2 = Me), **13-2** (R_1 = Et, R_2 = Me), **14-1** (R_1 = Ph, R_2 = Me), **14-2** (R_1 = Ph, R_2 = Me).

has been explained by incorporation of acetaldehyde. Finally we have determined that the reaction of *N*-fused porphyrin **2**, $SiMeHCl_2$, and acetone in pyridine afforded **8** as well. Altogether the described reaction leading to **8** is presented in Scheme 3.

NMR Studies of 8. The porphyrinoid **10** built into **8** is structurally related to the aromatic *N*-fused inner phlorin **11** (Chart 2) as both contain an identical macrocyclic frame and are differentiated merely by substitution at C(9).[31] Actually the macrocyclic structural motif of *N*-fused inner phlorin has been previously identified.[21,22]

Chart 2. *N*-Fused Inner Phlorin **11** and Its Acetone Derivative **10**[a]

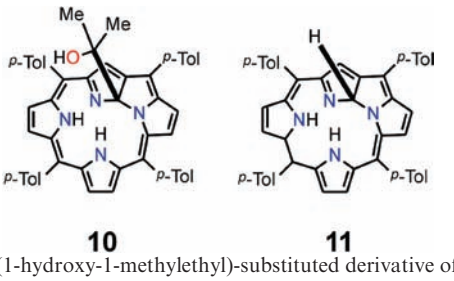

[a] The 9-(1-hydroxy-1-methylethyl)-substituted derivative of **11**.

Specifically a nucleophilic attack by alkoxides on boron *N*-fused porphyrin or an electrophilic attack by a hydrogen on phosphorus(V) *N*-fused isophlorin were previously applied to create an aromatic *N*-fused inner phlorin skeleton.

In the construction of the original structural model, the coordination of methylsilyl moiety to the three available nitrogens of *N*-fused inner phlorin has been considered as the starting point. Instead of H(9) the acetone derived bridging unit linked by oxygen to the silicon and the carbonyl carbon to C(9) has been incorporated. Altogether the formed species **8** remains neutral. The *syn* position of SiMe and C(9′)Me_2 (Scheme 3) results from the constraints imposed by the NMR as described below. The DFT studies been have been used to visualize the suggested structure of **8** and to assess the degree of the macrocycle distortion that is necessary to form such a structure (Figure 5).

The optimized structure of **8** highlights that the coordination polyhedron of silicon resembles the trigonal bipyramid. The macrocyclic ligand coordinates in the

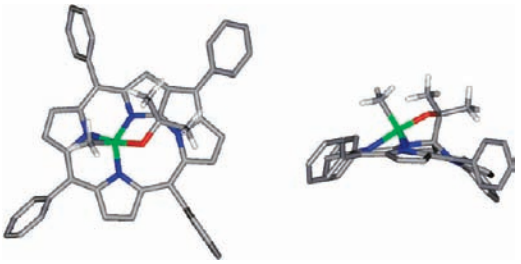

Figure 5. DFT optimized structure of **8** (left: perspective view; right: side view with aromatic hydrogens and *p*-Me groups removed for clarity).

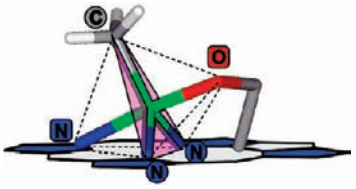

Figure 6. Trigonal bipyramid coordination sphere of silicon atom in **8**.

peculiar facial mode as the three pyrrolic nitrogen donors lie at the vertices of the single trigonal face (Figure 6).

Actually such an orientation of large cation coordination polyhedrons allows their coordination to tridentate macrocycles which provide a relatively small coordination crevice.[45−48] For instance an analogous coordination mode was observed for rhenium complexes of *N*-fused porphyrin[28,29] or for $[SiF_3(Me_3tacn)]Cl$, where a distorted octahedral cation built upon facially coordinated Me_3-tacn (*N*,*N*′,*N*″-trimethyl-1,4,7-triazacyclononane) and three fluoride ligands has been detected.[49] The meridional positions of the trigonal bipyramid of **8** are occupied by two pyrrolic nitrogen donors and a *σ*-methyl ligand. The coordination sphere is completed by apical coordination of the alkoxy oxygen atom derived from acetone which acts as an appended molecular side arm suitably built-in the unique acetone derivative of *N*-fused inner phlorin **10**. Consequently all methyl groups are adjacently located on the same side of the macrocyclic plane.

The straightforward assignment of SiMe resonance via $^1H-^{29}Si$ NMR scalar coupling (Figure 4, Inset A2) provided the initial step for the ^1H NMR analysis. The assignment of the methyl resonances has been also confirmed by synthesis of the selectively deuterated derivative **8**-d_6 where the CH_3 groups have been replaced by CD_3 ones as described above. Considering the spatial proximity of the 9′-Me(1) − *o*-H(10-anis) (3.36 Å) which contrasts with the large distance 9′-Me(2) − *o*-H(10-anis) (6.40 Å) as found at the DFT optimized structure of **8** one could expect the single NOE cross-peaks reflecting dipolar coupling bet;ween the single methyl of 9′-$(Me)_2$ and *o*-H(10-anisol) (in parentheses the shortest H−H distances are given). These structural features have been reflected in the NOESY map by a well-defined cross peak.

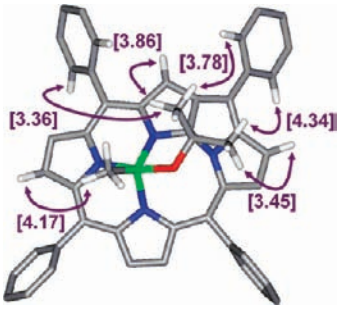

Figure 7. Established NOE connectivities for **8** (purple arrows). Only the analytically useful hydrogens are shown. Other hydrogens and *p*-Me groups are removed for clarity. The spatial proximities (in Å) are in parentheses.

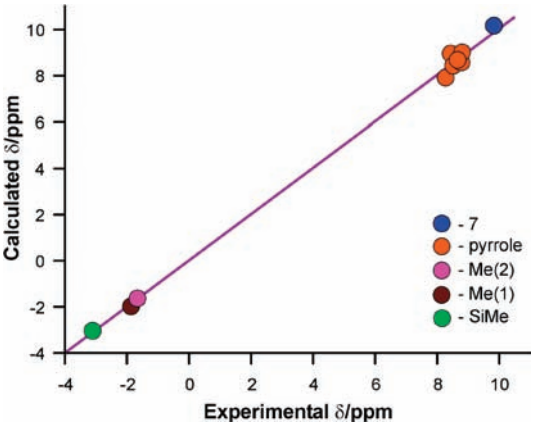

Figure 8. Linear correlation between calculated and experimental values of chemical shifts for **8**.

In addition the analysis of the DFT model reveals that the steric hindrance of the C(7)H and C(3)H fragments is smaller than that created by any other two *β*-CH couples flanking *meso*-anisoles as discussed above. This structural factor lowers the rotation barrier with respect to the C_{ipso}-C_{meso} bond in comparison to other *meso* positions, which results in the fast rotation of this substituent in the whole investigated 195−330 K temperature range presenting consistently the AA′BB′ spectroscopic pattern. On the contrary, as the temperature was gradually lowered all other anisole resonances broaden and eventually split into two signals reflecting the asymmetry with respect to the porphyrin plane (Figure 4). Actually the similar conformational flexibility was found characteristic for boron(III) and phosphorus(V) complexes of *N*-fused porphyrin derivatives.[21,22] This spectroscopic phenomenon provides an independent means to unambiguously identify the *meso*(5)-anisol resonances. Once assigned this particular set of resonances has been used as a starting point of NOE studies. The most fundamental steps are shown in Figure 7.

^1H NMR chemical shifts calculated for **8** using the GIAO B3LYP/6-31G** method are given in Supporting Information, Table S1. There is a satisfactory qualitative agreement for the available set of theoretical and experimental data readily demonstrated by linear correlations between the calculated and experimental chemical shifts as shown for the representative example of **8** (Figure 8).

(45) Wainwright, K. P. *Coord. Chem. Rev.* **1997**, *166*, 35–90.
(46) Gott, A. L.; McGovan, P. C.; Temple, C. N. *Organometallics* **2008**, *27*, 2852–2860.
(47) Romakh, V. B.; Therrien, B.; Suss-Fink, G.; Shul'pin, G. B. *Inorg. Chem.* **2007**, *46*, 3166–3175.
(48) Che, C. M.; Ho, C. M.; Huang, J. S. *Coord. Chem. Rev.* **2007**, *251*, 2145–2166.
(49) Cheng, F.; Hector, A. L.; Levason, W.; Reid, G.; Webster, M.; Zhang, W. J. *Chem. Commun.* **2009**, 1334–1336.

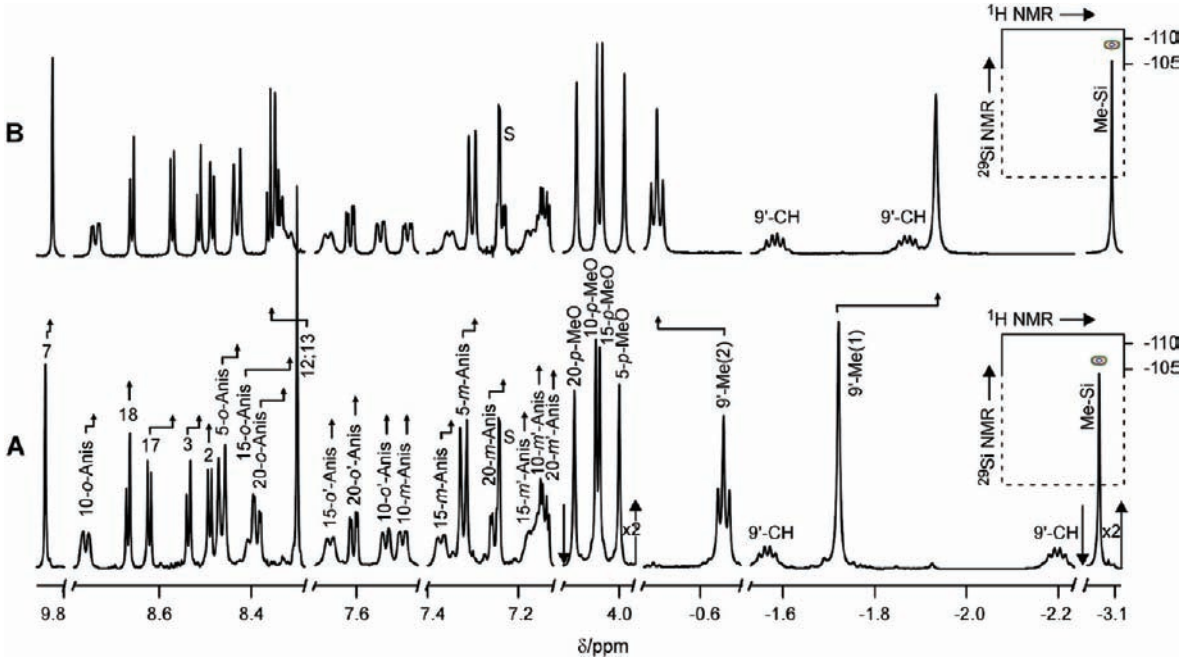

Figure 9. ^{1}H NMR spectra of (A) **13-2** and (B) **13-1** (chloroform-*d*, 210 K). Insets present ^{1}H−^{29}Si NMR correlations (chloroform-*d*, 298 K).

Significantly a combination of HMQC and HMBC correlations allowed an identification of a fused skeleton. The assignment of the C(9) and C(9′) resonances revealed the tetrahedral geometry consistent with the 89.9 and 76.6 ppm chemical shifts, respectively. In particular, the chemical shift of C(9) reflects the tetrahedral hybridization considering its substitution by two electronegative atoms and has been previously detected for phosphorus(V) *N*-fused inner phlorin.[21]

Addition of Aldehydes and Ketones. The reaction of *N*-confused porphyrin **1** with $SiMeHCl_2$ in triethylamine in the presence of aldehyde or ketone of choice afforded the analogous addition products as described already for acetone **8** or acetaldehyde **9-1** following the general reactivity route (Scheme 4). In addition to acetone and acetaldehyde the following compounds have been probed: acetophenone, butanone, propanal, benzaldehyde, *p*-methylbenzaldehyde, *p*-methoxybenzaldehyde, and terephthaldehyde affording after chromatography the analogues of **8**, **9-1**, or **9-2**, respectively, albeit the detailed analysis has been focused on four selected examples (each is a pair of stereoisomers **X-1** and **X-2**), that is, etanal **9**, propanal **12**, butanone **13**, and acetophenone **14**. The specific resonance assignments for **9-1**, **12- 1**, **13-1**, **13-2**, and **14-1** are shown in Figure 9 and Figure 12 and follows the methodology described in detail for **8** referring to details of the DFT optimized models (Supporting Information, Figure S2).

Apparently the addition of acetone resulted in formation of the NMR undistinguishable enantiomeric pair because of the single stereogenic C(9) carbon atom. All other ketones and aldehydes, used in this work, introduce the second stereogenic center because of the four different substituents at the C(9′) atom. In principle two enantiomeric pairs of diastereomers are expected to be differentiated and eventually identified by ^{1}H NMR. In fact the formation of two diastereomers has been observed in the single case of 2-butanone (Figure 9) where they have been

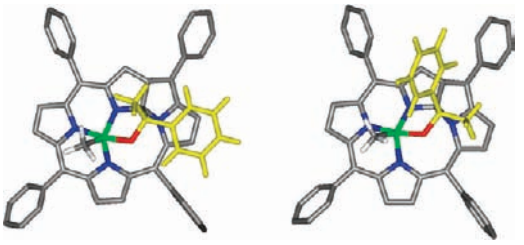

Figure 10. DFT optimized structure of **14-1** (left) and **14-2** (right). 1-Phenylethyl moiety derived from acetophenone in yellow. The macrocyclic hydrogens and *p*-Me groups are removed for clarity.

separated by column chromatography. This particular reaction is steroselective as clearly demonstrated by preference for **13-2**. Actually the **13-2** to **13-1** molar ratio equals 2:1. The methyl substituent of **13-2** is oriented toward N(21) (Scheme 4). Once the clear difference in bulkiness has been introduced ($R_2 \gg R_1$), which is the common feature for all explored aldehydes and acetophenone, the formation of the single stereoisomer (**9-1**, **12-1**, **14-1**) has been detected.

The analysis of the DFT optimized structures for each pair of diastereomers resulted in the conclusion that the steric strain imposed by R_1 and R_2 substituents may be of importance as a factor which determines the preference for the given stereoisomer. The representative analysis addresses the **14-1**−**14-2** couple (Figure 10). One can readily extract from the molecular structure of **14-1**−**14-2** the five-membered SiOC(9′)C(9)N(24) heterocycle (Figures 6 and 11), that is, the structural fragment which is crucial for the further discussion. The heterocyclic ring adopts a half chair conformation which is practically identical for both diastereomers. In particular the position of silicon and its methyl substituent remains conserved. However, depending on diastereomer the R_1 and R_2 substituents occupy axial and equatorial (**14-1**) or equatorial and axial positions (**14-2**) respectively

(Figure 11). Accordingly the energetically favorable trans arrangement of SiMe and phenyl substituent is expected for **14-1**. The cis arrangement of **14-2** imposes the larger steric transannular strain. Thus the distance of phenyl hydrogens to SiMe in **14-2** is close enough to result in efficient steric repulsion. In contrast the bulky equatorial phenyl group of **14-1** extends into space away from the SiMe group being replaced at the axial position by the smaller methyl of acetophenone.

The experimentally observed preference for formation of **9-1**, **12-1**, **14-1** and the coexistence of **13-1** and **13-2** species have raised the question of the relative stability of diastereomers. The DFT calculated total energies, using the B3LYP/6-31G**//B3LYP/6-31G** approach (Table 1) demonstrate that the stability of diastereomers is very similar. The energy difference between two diastereomers can be categorized as small (0.2 to 2.1 kcal/mol) once the intrinsic conformational flexibility of the structure is concerned. Actually only in the single case of the acetophenone adduct, the DFT calculations are consistent with the experimentally detected preference for **14-1**. Therefore, the stereoselective formation of diastereomers seems to indicate that the aldehyde or ketone addition is under kinetic but not thermodynamic control.

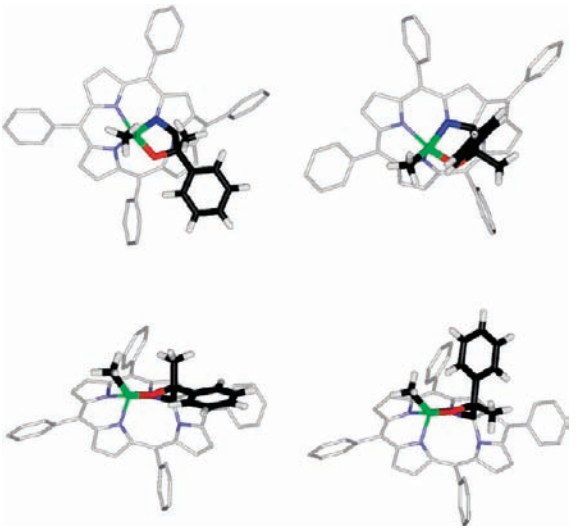

Figure 11. Heterocyles extracted from the DFT optimized structure of **14-1** (left) and **14-2** (right) (up: perspective views; down: side views). The macrocyclic hydrogens and *p*-Me groups removed for clarity.

Table 1. Relative Energies Calculated Using the B3LYP/6-31G**//B3LYP/6-31G**

derivatives of	compound	energies kcal/mol
acetaldehyde	**9-1**	0.49
	9-2	0
propanal	**12-1**	2.11
	12-2	0
butanone	**13-1**	0
	13-2	0.25
acetophenone	**14-1**	0
	14-2	2.10

^{1}H NMR chemical shifts calculated for **9-1**, **12-1**, **13-1**, **13-2**, **14-1** using the GIAO B3LYP/6-31G** method are given in Supporting Information, Tables S2−S6. There are satisfactory agreements for available sets of theoretical and experimental data readily demonstrated by linear correlations between the calculated and experimental chemical shifts (Supporting Information, Figures S6−S10). In particular, the two diastereoisomers **13-1** and **13-2** are recognizable with this methodology.

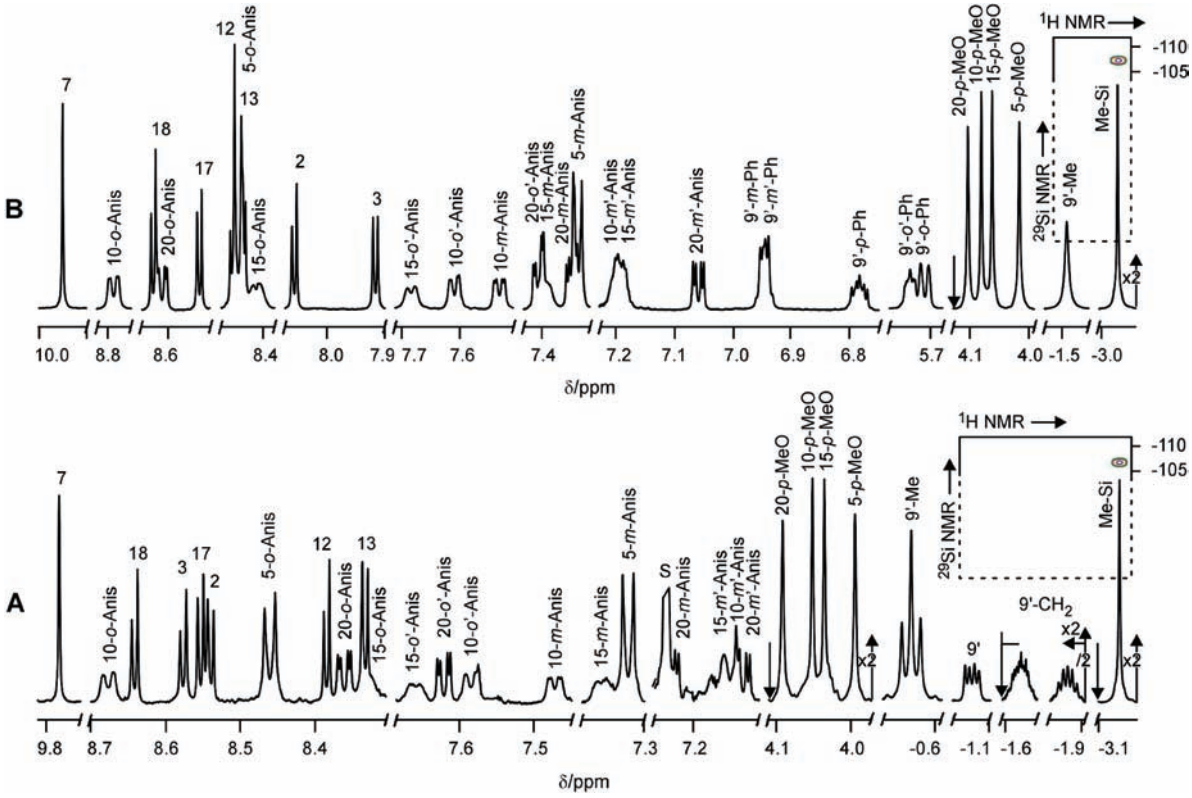

Figure 12. ^{1}H NMR spectra of (A) **12-1** and (B) **14-1** (chloroform-*d*, 210 K). Insets present ^{1}H−^{29}Si NMR correlations (chloroform-*d*, 298 K).

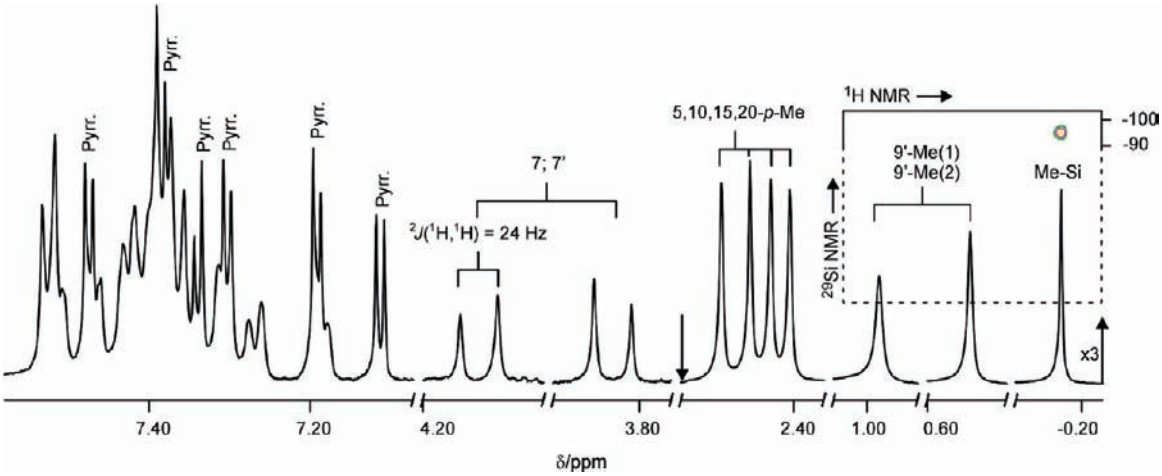

Figure 13. ^{1}H NMR spectrum of **15** with inset presenting ^{1}H−^{29}Si NMR correlation (dichloromethane-d_2, 230 K).

Scheme 5. Acidic Desililation of **8**

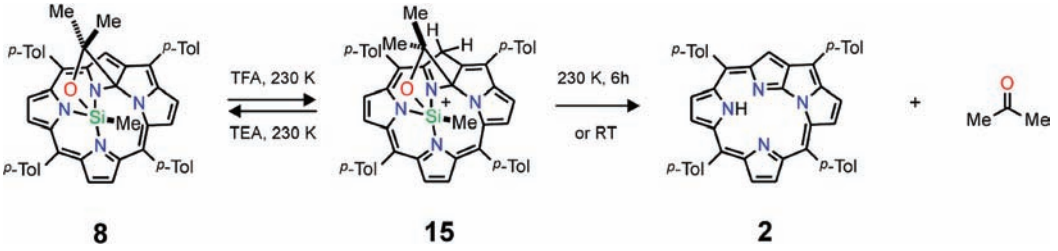

Chart 3. New Isomer of Tetraarylporphyrin

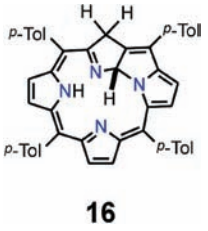

Desililation in the Presence of Acids. The systematic ^{1}H NMR titration of **8** in dichloromethane-d_2 carried out at 298 K, where the aliquots of dichloromethane-d_2 solution of trifluoroacetic acid (TFA) have been added, revealed that **8** undergoes instant desililation. The gradual decrease of resonances assigned to **8** has been accompanied by a rise of the *N*-fused porphyrin resonances which is formed as a sole macrocyclic product. An equimolar amount of acetone has been liberated as determined by integration. The identity of acetone has been confirmed by comparison to the ^{1}H NMR spectrum of this compound measured in identical conditions including acid concentration. Presumably the liberated silicon precipitates in the form of insoluble compounds.

Actually the acid triggered desililation is more complex as determined by ^{1}H NMR studies at 230 K. In the first step the protonation centers at the C(7) position affording **15** (Scheme 5). The reaction goes to completion once an equimolar amount of acid is added. The subsequent addition of nitrogen bases (pyridine, TEA) recovers the starting **8**. However, even at 230 K the gradual decay of **15** has been observed yielding directly *N*-fused porphyrin and acetone with a complete decomposition within 6 h.

Scheme 6. Acidic Desililation of **9**-1 (**12**-1)

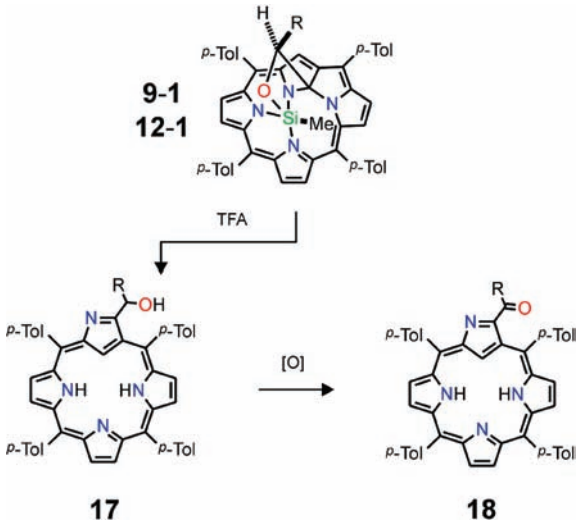

Predictably once the sample of **15** prepared at 230 K is warmed to 298 K the instantaneous decomposition takes place. The analogous reactivity toward acids has been determined for **14**-**1**. The ^{1}H NMR spectroscopic features of **15** reflect its non-aromaticity as the macrocyclic conjugated pathway of the maternal ring is interrupted because of the C(7) protonation. The C(7)H_2 group affords the remarkable AB pattern characterized by extremely large geminal coupling constant $^2J_{(H,H)}$ = 24 Hz (Figure 13). The ^{1}H NMR data collaborate with DFT optimized structure of **15** (Supporting Information, Figure S3).

We have also noticed that the macrocyclic structure of **15** imprints the molecular frame of the novel porphyrin

Scheme 7. Mechanism of Addition

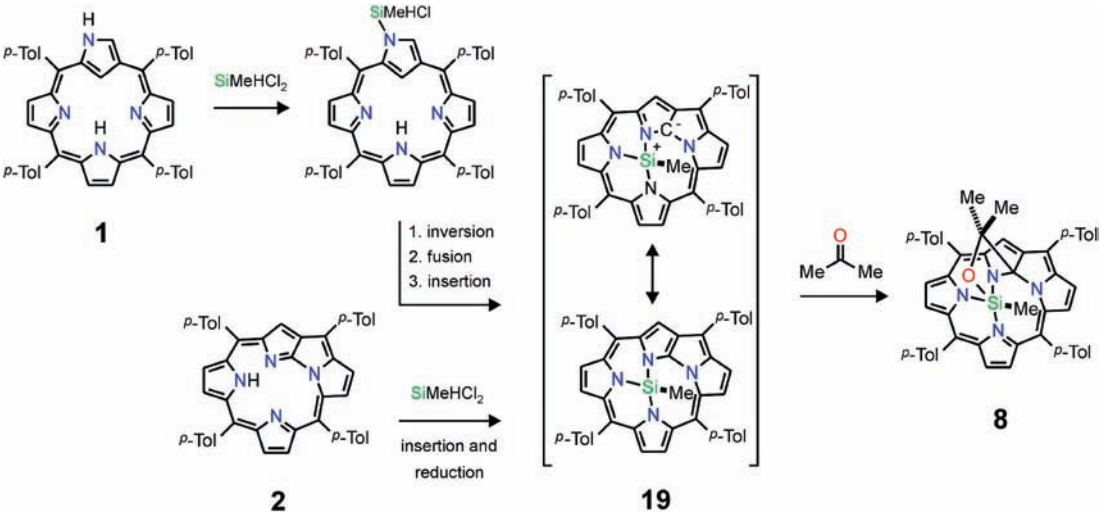

isomer **16** shown in Chart 3 adding to the collection of recently identified constitutional isomers of porphyrin which preserve the basic skeleton of their maternal *N*-fused porphyrin.[21,22]

In contrast to **8** and **14-1** compounds **9-1** and **12-1** which contain incorporated aldehyde moieties undergo a completely different transformation as shown at Scheme 6.

Namely, the addition of acid leads to desililation but accompanied by formation of two aromatic *N*-confused porphyrin derivatives, that is, 3-(1-hydroxyalkyl)-5,10,15,20-tetraaryl-2-aza-21-carbaporphyrin **17** and its oxidation product 3-alkanoyl-5,10,15,20-tetraaryl-2-aza-21-carbaporphyrin **18**. These macrocyclic products have been identified by comparison of the spectroscopic parameters reported already in the literature[43] as these species were previously synthesized applying an independent route. In striking contrast to **8** and **12-1**, the hydroxyalkyl and acyl moieties of **9**-1 and **12**-1 derived from aldehyde remain covalently attached preserving the C(9)-C(9′) bond. Thus the desililation prompts a profound intramolecular conversion of the *N*-fused porphyrin frame into *N*-confused porphyrin. Reinversion of *N*-fused porphyrin into *N*-confused porphyrin triggered by a methoxide was previously reported.[23] The low temperature studies on protonation of **9-1** and **12-1** have not identified any recognizable species formed by a feasible first step which might involve one proton addition.

Mechanism of Addition of Aldehyde or Ketone. Although the mechanistic picture of aldehyde or ketone addition still requires some experimental studies, we propose a plausible scenario illustrated here by the representative example of acetone. The formation of identical product starting from *N*-fused or *N*-confused porphyrin suggests the common intermediate which is formed in the course of the process to yield **8** (Scheme 7).

Thus the *N*-confused porphyrin **1** in pyridine (the dominating tautomer shown)[50,51] will readily react at the exposed external NH unit to afford **1**-SiMeHCl with a subsequent inversion of *N*-confused pyrrole ring. This rearrangement facilitates the next steps, that is, fusion and insertion accompanied by a release of HCl yielding transient **19**. At this stage of the reaction the methylsilicon(IV) is eventually coordinated to a trianionic tridentate ligand *N*-fused isophlorin (dihydro-*N*-fused porphyrin).[21,22] An alternative route involves the insertion of silicon(IV) to the *N*-fused porphyrin **2** accompanied by two electron reduction. It shows the crucial importance of the reductive properties of silane in this process. The *N*-fused isophlorin confined in **19** is prone to an electrophilic attack once the appropriate nucleophile is available. For instance phosphorus(V) *N*-fused isophlorin is susceptible to protonation at C(9) yielding two stereoisomers which are differentiated by location of the H(9) atom with respect to the oxygen atom of the PO unit.[21] A subsequent step (Scheme 7) involves nucleophilic attack of the carbonyl oxygen of acetone at the silicon center and C−C bond formation between the carbonyl carbon and the nucleophilic C(9) atom of *N*-confused isophlorin. Thus the reaction corresponds to the [3+2] annulation which combines the Si−N(23)−C(9) and the carbonyl group of acetone to shape the azaoxasilacyclopentane fragment.

Conclusion

Recently we have introduced silicon in the porphyrin-like structure aiming to replace one of the pyrrole fragments by silole.[52] The generated 21-silaphlorin related to phlorin derived from the [18]porphyrin(1.1.1.1) frame revealed a remarkable reactivity which involved an extrusion of a silylene unit followed by intramolecular rearrangements to form a non-aromatic *iso*-carbacorrole ring. In this work we have shown that two different modes of incorporation of silicon(IV) into the porphyrin-like structure can be explored starting from *N*-confused porphyrin. The first one resembles products of silicon insertion into the crevice of regular porphyrin affording the molecule with stretched N−Si or Si−O−C bonds. Alternatively, the reaction of *N*-confused porphyrin with silane triggered the peculiar rearrangements of *N*-confused porphyrin into isomeric *N*-fused phlorin

(50) Furuta, H.; Ishizuka, T.; Osuka, A.; Dejima, H.; Nakagawa, H.; Ishikawa, Y. *J. Am. Chem. Soc.* **2001**, *123*, 6207–6208.

(51) Pacholska, E.; Latos-Grażyński, L.; Szterenberg, L.; Ciunik, Z. *J. Org. Chem.* **2000**, *65*, 8188–8196.

(52) Skonieczny, J.; Latos-Grażyński, L.; Szterenberg, L. *Chem.—Eur. J.* **2008**, 4861–4874.

structure. The system must be stabilized via coordination of the side arm covalently linked to the inner C(9) carbon of the *N*-fused porphyrin skeleton created in situ by incorporation of aldehyde or ketone. Under such circumstances the high charge of silicon(IV) is compensated by the trianionic nature of the ligand.

It is of importance to make point here that both *N*-fused and *N*-confused porphyrins as ligands adjust their molecular structure and oxidation level to match both the charge and the size of the coordinated cation.[7,13,20−22,53,54] The suggested facial coordination of *N*-fused porphyrin derivatives is of particular importance here. Namely, a peculiar route to fit a cation to the limited size core of *N*-fused porphyrin via facial coordination of bispyramidal polyhedron has been appreciated suggesting a path for further exploration of coordination of *N*-fused porphyrin derivatives.[28,30,55,56]Actually this comment extends on the whole class tridentate contracted porphyrinoids including subporphyrins.[57−61] Importantly, this contribution has added a new isomeric structure to a large class of an emerging group of porphyrin isomers derived from *N*-fused porphyrin.[21,22]

Experimental Section

Materials. *meso*-Aryl substituted *N*-confused porphyrin **1**, *N*-fused porphyrin **2**, 21-hydroxy *N*-confused porphyrin **4** were obtained by previously described methods.[23,42,62] Dichloromethane, pyridine, and triethylamine were purified by standard procedures. Dichloromethylsilane, hexane, methanol, and all carbonyl compounds were used as received. All chromatographic separations were made on Silicagel 60 70−230 mesh.

3-Me. 5,10,15,20-tetra-(*p*-tolyl)-2-aza-21-carbaporphyrin **1** (30 mg (0.045 mmol)) was added to the 50 mL round-bottomed flask equipped with a stirring bar and heating coat and dissolved in 5 mL of freshly distilled CH_2Cl_2. Then 466 μL (4.5 mmol), a hundredfold excess, of dichloromethylsilane was added dropwise. The color of the solution has changed from brown-green to yellow-brown. After 5 min of intensive stirring at room temperature the reflux condenser was attached. Subsequently one 30 mL portion of triethylamine or pyridine was added. The solution color changed to light green. The solid of triethylammonum chloride precipitated and simultaneously the glassware was filled with white fumes. The reaction mixture was protected from moisture and refluxed for 2 h. During the process the color changed to dark green. The solution was slowly cooled to room temperature (1 h). The content of the flask was poured into 50 mL of hexane/dichloromethane (1:1 v/v). The resulting preliminary mixture was put on the top of a short chromatographic column (ca. 20 mL of dry bed + hexane/dichloromethane (1:1 v/v)), and 30 mL of dichloromethane was used to elute the product. The preliminary flash chromatography purified the products from solid of triethylamine and excess of reactive silane. The solvent was removed using a vacuum rotary evaporator. The yellow-green residue was dissolved in methanol/dichloromethane (1:99 v/v) and subjected to the proper chromatographic separation using a long column (ca. 40 mL of dry bed + methanol/dichloromethane (1:99 v/v)). The first very thin green fraction contained **8** and **9**-**1**. The second fraction eluted with methanol/dichloromethane (1.5:98.5 v/v) contained **3**-Me. The crude product was recrystallized with $CHCl_3$/MeOH. Yield of **3**-Me: 10 mg (31%). ^{1}H NMR (500 MHz, $CDCl_3$, 220 K): δ 8.75 (d, 1H, 13); 8.74 (d, 1H, 7); 8.72 (d, 1H, 8); 8.68 (d, 1H, 18); 8.41 (d, 1H, 20-*o*′-Tol); 8.21 (d, 1H, 5-*o*-Tol); 8.14 (d, 1H, 12); 8.13 (d, 1H, 17); 8.02 (s, 1H, 3); 7.98 (d, 1H, 15-*o*′-Tol); 7.93 (d, 1H, 10-*o*′-Tol); 7,81 (d, 1H, 10-*o*-Tol); 7.79 (m, 2H, 5-*o*′-Tol, 15-*o*-Tol); 7.65 (d, 1H, 20-*m*′-Tol); 7.61 (d, 1H, 20-*o*-Tol) 7.60 (d, 1H, 5-*m*-Tol) 7.54 (d, 1H, 15-*m*′-Tol); 7.53 (d, 1H, 10-*m*′-Tol); 7.50 (m, 2H, 10-*m*-Tol, 15-*m*-Tol); 7.47 (d, 1H, 5-*m*′-Tol); 7.45 (d, 1H, 20-*m*-Tol); 2.63 (s, 6H, 10-*p*-Me, 15-*p*-Me); 2.62 (s, 3H, 5-*p*-Me); 2.59 (s, 3H, 20-*p*-Me); −5.32 (s, 3H, Me-Si). ^{13}C NMR (126 MHz, $CDCl_3$, 220 K): δ 152.2 (3); 146.8 (11); 145.6 (9); 144.4 (16); 144.2 (6); 142.6 (14); 142.1 (19); 140.6, 136.5, 126.3 (1, 4, 21); 138.4 (C_4-5-Tol); 138.2 (C_4-20-Tol); 138.0 (C_1-20-Tol); 137.9 (C_4-10-Tol, C_4-15-Tol); 137.5 (C_1-5-Tol); 137.2 (5-*o*-Tol); 137.0 (C_1-10-Tol); 136.9 (C_1-15-Tol); 136.6, 133.3 (5-*o*′-Tol, 15-*o*-Tol); 136.2 (20-*o*-Tol, 20-*o*′-Tol); 134.9 (13); 134.1 (18); 133.6 (10-*o*′-Tol); 133.5 (15-*o*′-Tol); 133.3 (10-*o*-Tol); 133.2 (20); 131.6 (5); 130.6 (7); 129.8 (8); 128.5 (10-*m*-Tol, 15-*m*-Tol); 128.4 (10-*m*′-Tol, 15-*m*′-Tol); 128.3 (5-*m*-Tol); 128.1 (20-*m*-Tol, 5-*m*′-Tol); 127.9 (20-*m*′-Tol); 123.8 (12); 122.8 (17); 116.4 (15); 114.5 (10); 21.8 (10-*p*-Me, 15-*p*-Me, 20-*p*-Me); 21.7 (5-*p*-Me); 0.5 (Me-Si). ^{29}Si NMR (99 MHz, $CDCl_3$, 298 K): δ −108.0. HRMS (EI): *m*/*z* calcd for $C_{49}H_{39}N_4OSi$: 727.2888, found: 727.2812 $[M+H]^+$. UV−vis (CH_2Cl_2, 298 K): λ_{max} (log ε) = 448 (6.00), 476 (5.53), 561 (4.74), 612 (4.82), 671 (4.76), 723 nm (4.61).

6. The insertion of silicon(IV) into 2-methyl-5,10,15,20-tetra-(*p*-tolyl)-2-aza-21-hydroxy-21-carbaporphyrin followed the procedure described for **3**-Me. Yield of **6**: 8 mg (24%). ^{1}H NMR (500 MHz, $CDCl_3$, 250 K): δ 8.92 (d, 1H, 13); 8.84 (2d, 2H, 7, 12); 8.51 (d, 1H, 18); 8.32 (d, 1H, 8); 8.30 (d, 1H, 20-*o*-Tol); 8.27 (d, 1H, 17); 8.22 (d, 1H, 5-*o*-Tol); 8.07 (d, 1H, 15-*o*-Tol); 7.96 (d, 1H, 10-*o*-Tol); 7.91 (d, 1H, 10-*o*-Tol); 7.82 (d, 1H, 15-*o*-Tol); 7.74 (d, 1H, 5-*o*-Tol); 7.69 (d, 1H, 20-*o*-Tol); 7.59 (d, 1H, 5-*m*-Tol); 7.58 (d, 1H, 5-*m*-Tol); 7.56 (d, 1H, 15-*m*-Tol); 7.54 (d, 1H, 10-*m*-Tol); 7.53 (d, 1H, 10-*m*-Tol); 7.52 (d, 1H, 20-*m*-Tol); 7.50 (d, 1H, 15-*m*-Tol); 7.46 (d, 1H, 20-*m*-Tol); 2.94 (s, 3H, Me-N); 2.66 (s, 3H, 10-*p*-Me); 2.65 (2s, 6H, 5-*p*-Me, 15-*p*-Me); 2.62 (s, 3H, 20-*p*-Me); −5.57 (s, 3H, Me-Si). ^{13}C NMR (126 MHz, $CDCl_3$, 250 K): δ 164.1 (3); 146.0 (9); 145.4 (11); 144.5 (6); 144.0 (19); 141.8 (14); 141.1 (16); 139.3 (C_4-5-Tol); 138.6 (C_4-20-Tol); 138.4 (C_1-20-Tol); 137.9 (C_1-15-Tol); 137.8 (C_1-10-Tol); 137.7 (C_1-5-Tol); 137.5 (C_4-10-Tol); 137.3 (C_4-15-Tol); 136.9, 117.8 (4, 21); 135.0 (20-*o*-Tol); 134.6, 127.8 (7, 12); 134.2 (5-*o*-Tol); 133.9 (10-*o*-Tol); 133.7 (15-*o*-Tol, 20-*o*-Tol); 133.5 (10-*o*-Tol, 15-*o*-Tol); 132.6 (1); 131.4 (18); 130.1 (13); 128.6 (5-*m*-Tol, 10-*m*-Tol); 128.44 (5-*m*-Tol); 128.37 (15-*m*-Tol); 128.33 (10-*m*-Tol); 128.27 (20-*m*-Tol); 128.2 (5); 127.8 (20-*m*-Tol); 124.4 (8); 122.9 (17); 118.7 (20); 117.9 (15); 113.3 (10); 29.5 (Me-N); 21.8 (5-*p*-Me, 10-*p*-Me, 15-*p*-Me, 20-*p*-Me); −0.6 (Me-Si). ^{29}Si NMR (99 MHz, $CDCl_3$, 298 K): δ −112.0. HRMS (EI): *m*/*z* calcd for $C_{50}H_{41}N_4O_2Si^+$: 757.3004, found: 757.3010 $[M+H]^+$. UV−vis (CH_2Cl_2, 298 K): λ_{max} (log ε) = 451 (6.94), 480 (6.72), 565 (6.15), 618 (6.34), 656 (6.03), 679 nm (5.99).

8. 5,10,15,20-tetrakis(*p*-methoxyphenyl)-2-aza-21-carbaporphyrin **1** (30 mg (0.041 mmol)) was added to the 50 mL round-bottomed flask equipped with a stirring bar and heating

(53) Pawlicki, M.; Latos-Grażyński, L. *Chem.—Eur. J.* **2003**, *9*, 4650–4660.
(54) Pawlicki, M.; Latos-Grażyński, L. *J. Org. Chem.* **2005**, *70*, 9123–9130.
(55) Berlicka, A.; Latos-Grażyński, L.; Lis, T. *Angew. Chem., Int. Ed.* **2005**, *44*, 5288–5291.
(56) Berlicka, A.; Sprutta, N.; Latos-Grażyński, L. *Chem. Commun.* **2006**, 3346–3348.
(57) Myśliborski, R.; Latos-Grażyński, L.; Szterenberg, L.; Lis, T. *Angew. Chem., Int. Ed.* **2006**, *45*, 3670–3674.
(58) Inokuma, Y.; Yoon, Z. S.; Kim, D.; Osuka, A. *J. Am. Chem. Soc.* **2007**, *129*, 4747–4761.
(59) Saito, S.; Kim, K. S.; Yoon, Z. S.; Kim, D.; Osuka, A. *Angew. Chem., Int. Ed.* **2007**, *46*, 5591–5593.
(60) Inokuma, Y.; Kwon, J. H.; Ahn, T. K.; Yoo, M.-C.; Kim, D.; Osuka, A. *Angew. Chem., Int. Ed.* **2006**, *45*, 961–964.
(61) Takeuchi, Y.; Matsuda, A.; Kobayashi, N. *J. Am. Chem. Soc.* **2007**, *129*, 8271–8281.
(62) Geier, G. R. III; Haynes, D. M.; Lindsey, J. S. *Org. Lett.* **1999**, *1*, 1455–1458.

coat and dissolved in 5 mL of freshly distilled CH_2Cl_2. Acetone (3.1 μL, 0.041 mmol) was added. Subsequently dichloromethylsilane (425 μL (4.1 mmol), a hundredfold excess) was added dropwise. The color of the solution has changed from brown-green to yellow-brown. After 5 min of intensive stirring at room temperature the reflux condenser was attached. Subsequently one 30 mL portion of triethylamine was added. The solution color changed to light green. The solid of triethylammonum chloride precipitated and simultaneously the glassware was filled with white fumes. The reaction mixture was protected from moisture and refluxed for 2 h During the process the color changed to dark green. The solution was slowly cooled to room temperature (1 h). The content of flask was poured into 50 mL of hexane/dichloromethane (1:1 v/v). The resulting mixture preliminary was put on the top of a short chromatographic column (ca. 20 mL of dry bed + hexane/dichloromethane (1:1 v/v)), and 30 mL of dichloromethane was used to elute the product. The preliminary flash chromatography purified the products from solid of triethylamine and excess of reactive silane. The solvent was removed using a vacuum rotary evaporator. The yellow-green residue was dissolved in methanol/dichloromethane (1:99 v/v) and subjected to the proper chromatographic separation using a long column (ca. 40 mL of dry bed + methanol/dichloromethane (1:99 v/v)). The acetone derivative **8** was eluted as the first green fraction. The second fraction eluted with methanol/dichloromethane (1.5:98.5 v/v) contained **3**-Me. The crude product was recrystallized with CH_2Cl_2/MeOH. Yield of **8**: 5 mg (14%). ^{1}H NMR (600 MHz, $CDCl_3$, 210 K): δ 9.86 (s, 1H, 7); 8.74 (d, 1H, 10-*o*-Anis); 8.68 (d, 1H, 18); 8.65 (d, 1H, 17); 8.56 (d, 1H, 3); 8.52 (d, 1H, 2); 8.49 (d, 2H, 5-*o*-Anis); 8.40, (2d, 2H, 15-*o*-Anis, 20-*o*-Anis); 8.35 (d, 1H, 12); 8.33 (d, 1H, 13); 7.69 (d, 1H, 15-*o*′-Anis); 7.63 (d, 1H, 20-*o*′-Anis); 7.57 (d, 1H, 10-*o*‘-Anis); 7.50 (d, 1H, 10-*m*-Anis); 7.38 (d, 1H, 15-*m*-Anis); 7.33 (d, 2H, 5-*m*-Anis); 7.25 (d, 1H, 20-*m*-Anis); 7.19 (d, 1H, 15-*m*′-Anis); 7.17 (d, 1H, 10-*m*′-Anis); 7.15 (d, 1H, 20-*m*′-Anis); 4.10 (s, 3H, 20-*p*-MeO); 4.06 (s, 3H, 10-*p*-MeO); 4.05 (s, 3H, 15-*p*-MeO); 4.01 (s, 3H, 5-*p*-MeO); −1.65 (s, 3H, 9′-Me(2)); −1.84 (s, 3H, 9′-Me(1)); −3.09 (s, 3H, Me-Si). ^{13}C NMR (151 MHz, $CDCl_3$, 210 K): δ 158.9 (C_4-15-Anis); 158.7 (C_4-5-Anis, C_4-10-Anis); 158.4 (C_4-20-Anis); 154.9, 150.7 (6, 8); 148.2 (14); 148.1 (4); 146.4 (19); 142.9 (16); 140.9 (11); 139.4 (C_1-20-Anis); 138.7 (2); 135.7 (1); 135.6 (15-*o*-Anis); 135.3 (10-*o*-Anis); 135.0 (10-*o*′-Anis); 134.6 (20-*o*-Anis, 15-*o*′-Anis); 134.2 (20-*o*′-Anis); 133.8 (18); 131.8 (5-*o*-Anis); 131.1 (C_1-15-Anis); 130.7 (C_1-10-Anis); 128.1 (C_1-5-Anis); 126.7 (13); 124.6 (12); 122.8 (17); 120.4 (5); 119.4 (15); 118.9 (20); 115.1 (5-*m*-Anis, 7); 115.1 (5-*m*-Anis); 113.7 (10-*m*′-Anis); 113.6 (3, 10, 10-*m*-Anis); 113.3 (15-*m*′-Anis); 113.0 (15-*m*-Anis); 112.1 (20-*m*′-Anis); 110.5 (20-*m*-Anis); 89.9 (9); 76.6 (9′); 55.84 (5-*p*-MeO); 55.76 (10-*p*-MeO, 15-*p*-MeO, 20-*p*-MeO); 21.6 (9′-Me(1)); 16.2 (9′-Me(2)); 0.6 (Me-Si). ^{29}Si NMR (99 MHz, $CDCl_3$, 298 K): δ −107.2. HRMS (EI): *m*/*z* calcd for $C_{52}H_{45}N_4O_5Si^+$: 833.3165, found: 833.3171 $[M+H]^+$. UV−vis (CH_2Cl_2, 298 K): λ_{max} (log ε) = 471 (5.79), 500 (5.61), 656 (5.25), 697 nm (4.97).

9-1, 12-1, 13-1, 13-2, 14-1. The synthesis of the carbonyl adducts followed the procedure described for **8**.

9-1. Yield of **9-1**: 5 mg (16%). ^{1}H NMR (600 MHz, $CDCl_3$, 210 K): δ 9.80 (s, 1H, 7); 8.68 (d, 1H, 10-*o*-Anis); 8.66 (d, 1H, 18); 8.62 (d, 1H, 17); 8.59 (d, 1H, 3); 8.56 (d, 1H, 2); 8.49 (d, 2H, 5-*o*-Anis); 8.38 (d, 1H, 15-*o*-Anis); 8.36 (d, 1H, 20-*o*-Anis); 8.34 (d, 1H, 13); 8.31 (d, 1H, 12); 7.66 (d, 1H, 15-*o*′-Anis); 7.64 (d, 1H, 20-*o*′-Anis); 7.58 (d, 1H, 10-*o*′-Anis); 7.48 (d, 1H, 10-*m*-Anis); 7.38 (d, 1H, 15-*m*-Anis); 7.32 (d, 2H, 5-*m*-Anis); 7.24 (d, 1H, 20-*m*-Anis); 7.17 (d, 1H, 15-*m*′-Anis); 7.16 (d, 1H, 10-*m*′-Anis); 7.14 (d, 1H, 20-*m*′-Anis); 4.10 (s, 3H, 20-*p*-MeO); 4.05 (s, 3H, 10-*p*-MeO); 4.04 (s, 3H, 15-*p*-MeO); 4.00 (s, 3H, 5-*p*-MeO); −0.81 (q, 1H, 9′); −1.78 (d, 3H, 9′-Me); −3.14 (s, 3H, Me-Si). ^{13}C NMR (151 MHz, $CDCl_3$, 210 K): δ 158.7 (C_4-15-Anis); 158.4 (C_4-5-Anis, C_4-10-Anis); 158.3 (C_4-20-Anis); 155.4, 150.9 (6, 8); 148.0, 140.5 (11, 14); 147.7 (4); 146.6 (19); 142.7 (16); 139.2 (C_1-20-Anis); 138.5 (2); 135.8 (1); 135.4 (15-*o*-Anis); 134.9 (10-*o*-Anis, 10-*o*′-Anis); 134.4 (20-*o*-Anis); 134.3 (15-*o*′-Anis); 134.0 (20-*o*′-Anis); 133.6 (18); 131.6 (5-*o*-Anis); 131.0 (C_1-15-Anis); 130.6 (C_1-10-Anis); 128.0 (C_1-5-Anis); 126.7 (13); 124.9 (12); 122.3 (17); 120.6 (5); 119.8 (15); 118.9 (20); 115.0 (5-*m*-Anis); 113.6 (3); 113.5 (10); 113.2 (10-*m*-Anis, 10-*m*′-Anis); 113.0 (15-*m*′-Anis); 112.9 (7); 112.8 (15-*m*-Anis); 111.7 (20-*m*′-Anis); 110.4 (20-*m*-Anis); 90.3 (9); 72.0 (9′); 55.6 (5-*p*-MeO); 55.5 (10-*p*-MeO, 15-*p*-MeO, 20-*p*-MeO); 9.7 (9′-Me); −1.3 (Me-Si). ^{29}Si NMR (99 MHz, $CDCl_3$, 298 K): δ −108.1. HRMS (EI): *m*/*z* calcd for $C_{51}H_{43}N_4O_5Si^+$: 819.3008, found: 819.3004 $[M+H]^+$. UV−vis (CH_2Cl_2, 298 K): λ_{max} (log ε) = 472 (5.84), 499 (5.66), 656 (5.24), 694 nm (4.90).

12-1. Yield of **12-1**: 3 mg (9%). ^{1}H NMR (600 MHz, $CDCl_3$, 210 K): δ 9.78 (s, 1H, 7); 8.68 (d, 1H, 10-*o*-Anis); 8.64 (d, 1H, 18); 8.58 (d, 1H, 3); 8.55 (d, 1H, 17); 8.54 (d, 1H, 2); 8.46 (d, 2H, 5-*o*-Anis); 8.38 (d, 1H, 12); 8.36 (d, 1H, 20-*o*-Anis); 8.33 (d, 1H, 13); 8.32 (br, 1H, 15-*o*-Anis); 7.66 (d, 1H, 15-*o*′-Anis); 7.62 (d, 1H, 20-*o*′-Anis); 7.58 (d, 1H, 10-*o*′-Anis); 7.47 (d, 1H, 10-*m*-Anis); 7.36 (d, 1H, 15-*m*-Anis); 7.32 (d, 2H, 5-*m*-Anis); 7.23 (d, 1H, 20-*m*-Anis); 7.17 (d, 1H, 15-*m*′-Anis); 7.15 (d, 1H, 10-*m*′-Anis); 7.14 (d, 1H, 20-*m*′-Anis); 4.09 (s, 3H, 20-*p*-MeO); 4.05 (s, 3H, 10-*p*-MeO); 4.04 (s, 3H, 15-*p*-MeO); 3.99 (s, 3H, 5-*p*-MeO); −0.56 (t, 3H, 9′-Me); −1.05 (m, 1H, 9′); −1.64, −1.86 (2m, 2H, 9′-CH_2); −3.13 (s, 3H, Me-Si). ^{13}C NMR (151 MHz, $CDCl_3$, 210 K): δ 158.7 (C_4-15-Anis); 158.4 (C_4-10-Anis); 158.3 C_4-5-Anis); 158.2 (C_4-20-Anis); 155.3, 149.3 (6, 8); 148.3 (14); 148.0 (4); 146.3 (19); 142.6 (16); 140.1 (11); 139.2 (C_1-20-Anis); 138.4 (2); 135.2 (15-*o*-Anis); 134.8 (10-*o*-Anis); 134.7 (10-*o*′-Anis); 134.4 (1); 134.2 (20-*o*-Anis); 134.0 (15-*o*′-Anis); 133.7 (20-*o*′-Anis); 133.3 (18); 131.5 (5-*o*-Anis); 131.0 (C_1-15-Anis); 130.6 (C_1-10-Anis); 127.8 (C_1-5-Anis); 126.5 (12); 124.8 (13); 122.0 (17); 119.9 (20); 119.8 (5); 119.6 (15); 114.9 (5-*m*-Anis); 114.3 (10); 113.2 (10-*m*-Anis); 113.1 (10-*m*′-Anis, 15-*m*′-Anis); 112.9 (3, 7); 112.7 (15-*m*-Anis); 111.6 (20-*m*′-Anis); 110.4 (20-*m*-Anis); 88.9 (9); 78.5 (9′); 55.6 (5-*p*-MeO, 10-*p*-MeO, 15-*p*-MeO, 20-*p*-MeO); 17.4 (9′-CH_2); 8.9 (9′-Me); −1.9 (Me-Si). ^{29}Si NMR (99 MHz, $CDCl_3$, 298 K): δ −108.1. HRMS (EI): *m*/*z* calcd for $C_{52}H_{45}N_4O_5Si^+$: 833.3165, found: 833.3140 $[M+H]^+$. UV−vis (CH_2Cl_2, 298 K): λ_{max} (log ε) = 474 (5.85), 499 (5.67), 655 (5.26), 697 nm (4.98).

13-1. The butanone derivatives were eluted as two fastest moving green fractions. The first fraction contained **13-1** and the second one **13-2**. Yield of **13-1**: 2 mg (7%). ^{1}H NMR (600 MHz, $CDCl_3$, 210 K): δ 9.82 (s, 1H, 7); 8.74 (d, 1H, 10-*o*-Anis); 8.66 (d, 1H, 18); 8.57 (d, 1H, 17); 8.51 (d, 1H, 3); 8.48 (d, 1H, 2); 8.43 (d, 2H, 5-*o*-Anis); 8.36 (d, 1H, 12); 8.34 (d, 1H, 13); 8.33 (d, 1H, 20-*o*-Anis); 8.32 (d, 1H, 15-*o*-Anis); 7.66 (d, 1H, 15-*o*′-Anis); 7.61 (d, 1H, 20-*o*′-Anis); 7.55 (d, 1H, 10-*o*′-Anis); 7.49 (d, 1H, 10-*m*-Anis); 7.35 (d, 1H, 15-*m*-Anis); 7.30 (d, 2H, 5-*m*-Anis); 7.23 (d, 1H, 20-*m*-Anis); 7.17 (d, 1H, 15-*m*′-Anis); 7.15 (d, 1H, 10-*m*′-Anis); 7.14 (d, 1H, 20-*m*′-Anis); 4.09 (s, 3H, 20-*p*-MeO); 4.05 (s, 3H, 10-*p*-MeO); 4.04 (s, 3H, 15-*p*-MeO); 3.99 (s, 3H, 5-*p*-MeO); −0.50 (t, 3H, 9′-Me(2)); −1.58, −1.87 (2m, 2H, 9′-CH_2); −1.93 (s, 3H, 9′-Me(1)); −3.09 (s, 3H, Me-Si). ^{13}C NMR (151 MHz, $CDCl_3$, 210 K): δ 158.7 (C_4-15-Anis); 158.4 (C_4-5-Anis, C_4-10-Anis); 158.3 (C_4-20-Anis); 155.4, 150.9 (6, 8); 148.0, 140.5 (11, 14); 147.7 (4); 146.6 (19); 142.7 (16); 139.2 (C_1-20-Anis); 138.2 (2); 135.8 (1); 135.2 (15-*o*-Anis); 135.1 (10-*o*-Anis); 134.8 (10-*o*′-Anis); 134.6 (20-*o*-Anis); 134.2 (15-*o*′-Anis); 133.8 (20-*o*′-Anis); 133.2 (18); 131.6 (5-*o*-Anis); 131.0 (C_1-15-Anis); 130.6 (C_1-10-Anis); 128.0 (C_1-5-Anis); 126.5, 124.4 (12, 13); 122.4 (17); 120.6 (5); 119.8 (15); 118.9 (20); 115.3 (7); 114.9 (5-*m*-Anis); 113.5 (10); 113.4 (10-*m*-Anis, 10-*m*′-Anis); 113.0 (3, 15-*m*′-Anis); 112.8 (15-*m*-Anis); 111.6 (20-*m*′-Anis); 110.4 (20-*m*-Anis); 90.3 (9); 79.4 (9′); 55.7 (5-*p*-MeO); 55.5 (10-*p*-MeO, 15-*p*-MeO, 20-*p*-MeO); 21.2 (9′-CH_2); 17.2 (9′-Me(1)); 7.4 (9′-Me(2)); 0.4 (Me-Si). ^{29}Si NMR (99 MHz, $CDCl_3$, 298 K):

δ −107.5. HRMS (EI): m/z calcd for $C_{53}H_{47}N_4O_5Si^+$: 847.3321, found: 847.3340 $[M+H]^+$. UV−vis (CH_2Cl_2, 298 K): λ_{max} (log ε) = 472 (6.05), 502 (5.87), 659 (5.47), 698 nm (5.18).

13-2. The butanone derivatives were eluted as the two fastest moving green fractions. The first fraction contained **13-1** and the second one **13-2**. Yield of **13-2**: 5 mg (14%). ^{1}H NMR (600 MHz, $CDCl_3$, 210 K): δ 9.84 (s, 1H, 7); 8.76 (d, 1H, 10-*o*-Anis); 8.67 (d, 1H, 18); 8.62 (d, 1H, 17); 8.54 (d, 1H, 3); 8.49 (d, 1H, 2); 8.46 (d, 2H, 5-*o*-Anis); 8.40 (d, 1H, 15-*o*-Anis); 8.39 (d, 1H, 20-*o*-Anis); 8.30 (s, 2H, 12, 13); 7.66 (d, 1H, 15-*o*′-Anis); 7.60 (d, 1H, 20-*o*′-Anis); 7.54 (d, 1H, 10-*o*′-Anis); 7.50 (d, 1H, 10-*m*-Anis); 7.37 (d, 1H, 15-*m*-Anis); 7.32 (d, 2H, 5-*m*-Anis); 7.25 (d, 1H, 20-*m*-Anis); 7.17 (d, 1H, 15-*m*′-Anis); 7.15 (d, 1H, 10-*m*′-Anis); 7.14 (d, 1H, 20-*m*′-Anis); 4.10 (s, 3H, 20-*p*-MeO); 4.05 (s, 3H, 10-*p*-MeO); 4.04 (s, 3H, 15-*p*-MeO); 4.00 (s, 3H, 5-*p*-MeO); −0.65 (t, 3H, 9′-Me(2)); −1.56, −2.20 (2m, 2H, 9′-CH_2); −1.72 (s, 3H, 9′-Me(1)); −3.07 (s, 3H, Me-Si). ^{13}C NMR (151 MHz, $CDCl_3$, 210 K): δ 158.7 (C_4-15-Anis); 158.5 (C_4-5-Anis); 158.4 (C_4-10-Anis); 158.2 (C_4-20-Anis); 155.0, 150.5 (6, 8); 148.2, 140.9 (11, 14); 148.0 (4); 146.4 (19); 142.7 (16); 139.2 (C_1-20-Anis); 138.2 (2); 135.9 (1); 135.5 (15-*o*-Anis); 135.1 (10-*o*-Anis); 134.9 (10-*o*′-Anis); 134.3 (20-*o*-Anis, 15-*o*′-Anis); 134.0 (20-*o*′-Anis); 133.5 (18); 131.7 (5-*o*-Anis); 131.0 (C_1-15-Anis); 130.5 (C_1-10-Anis); 128.0 (C_1-5-Anis); 126.6, 124.3 (12, 13); 122.3 (17); 120.2 (5); 119.3 (15); 118.5 (20); 115.5 (5-*m*-Anis); 114.9 (7); 113.5 (10); 113.4 (10-*m*-Anis); 113.3 (10-*m*′-Anis); 113.2 (3, 15-*m*′-Anis); 112.8 (15-*m*-Anis); 111.8 (20-*m*′-Anis); 110.3 (20-*m*-Anis); 90.1 (9); 79.6 (9′); 55.6 (5-*p*-MeO); 55.5 (10-*p*-MeO, 15-*p*-MeO, 20-*p*-MeO); 25.9 (9′-CH_2); 11.8 (9′-Me(2)); 7.3 (9′-Me(1)); 0.4 (Me-Si). ^{29}Si NMR (99 MHz, $CDCl_3$, 298 K): δ −107.4. HRMS (EI): m/z calcd for $C_{53}H_{47}N_4O_5Si^+$: 847.3321, found: 847.3340 $[M+H]^+$. UV−vis (CH_2Cl_2, 298 K): λ_{max} (log ε) = 472 (6.04), 500 (5.83), 657 (5.44), 695 nm (5.17).

14-1. Yield of **14-1**: 4 mg (11%). ^{1}H NMR (600 MHz, $CDCl_3$, 210 K): δ 9.95 (s, 1H, 7); 8.78 (d, 1H, 10-*o*-Anis); 8.62 (d, 1H, 18); 8.60 (d, 1H, 20-*o*-Anis); 8.54 (d, 1H, 17); 8.44 (d, 1H, 12); 8.43 (d, 2H, 5-*o*-Anis); 8.42 (d, 1H, 13); 8.40 (d, 1H, 15-*o*-Anis); 8.05 (d, 1H, 2); 7.91 (d, 1H, 3); 7.67 (d, 1H, 15-*o*′-Anis); 7.60 (d, 1H, 10-*o*′-Anis); 7.52 (d, 1H, 10-*m*-Anis); 7.40 (d, 1H, 20-*o*′-Anis); 7.38 (d, 1H, 15-*m*-Anis); 7.34 (d, 1H, 20-*m*-Anis); 7.33 (d, 2H, 5-*m*-Anis); 7.20 (d, 1H, 10-*m*′-Anis); 7.18 (d, 1H, 15-*m*′-Anis); 7.05 (d, 1H, 20-*m*′-Anis); 6.94 (m, 1H, 9′-*m*-Ph); 6.93 (m, 1H, 9′-*m*′-Ph); 6.78 (m, 1H, 9′-*p*-Ph); 5.72 (m, 1H, 9′-*o*′-Ph); 5.70 (d, 1H, 9′-*o*-Ph); 4.10 (s, 3H, 20-*p*-MeO); 4.07 (s, 3H, 10-*p*-MeO); 4.05 (s, 3H, 15-*p*-MeO); 4.01 (s, 3H, 5-*p*-MeO); −1.52 (d, 3H, 9′-Me); −3.04 (s, 3H, Me-Si). ^{13}C NMR (151 MHz, $CDCl_3$, 210 K): δ 158.6 (C_4-5-Anis); 158.5 (C_4-10-Anis, C_4-15-Anis); 158.1 (C_4-20-Anis); 154.1, 150.7 (6, 8); 147.6 (14); 148.0 (4); 146.1 (19); 142.8 (16); 140.2 (11); 139.3 (C_1-20-Anis); 139.0 (2); 135.6 (C_1-9′-Ph); 135.1 (10-*o*-Anis, 15-*o*-Anis); 134.8 (10-*o*′-Anis); 134.6 (20-*o*-Anis, 20-*o*′-Anis); 134.5 (1); 134.2 (15-*o*′-Anis); 133.0 (17); 131.9 (5-*o*-Anis); 130.8 (C_1-15-Anis); 130.5 (C_1-10-Anis); 128.8 (C_1-5-Anis); 126.3 (9′-*o*′-Ph, 12); 126.2 (9′-*m*-Ph); 125.6 (9′-*p*-Ph); 125.2 (9′-*m*′-Ph); 124.5 (13); 123.9 (9′-*o*-Ph); 122.4 (18); 121.2 (5); 118.6 (20); 118.4 (15); 115.3 (7); 114.9 (5-*m*-Anis); 113.5 (10); 113.4 (10-*m*-Anis); 113.2 (10-*m*′-Anis, 15-*m*′-Anis); 112.9 (3); 112.7 (15-*m*-Anis); 111.7 (20-*m*′-Anis); 110.5 (20-*m*-Anis); 90.1 (9); 80.1 (9′); 55.6 (5-*p*-MeO, 10-*p*-MeO, 15-*p*-MeO, 20-*p*-MeO); 22.5 (9′-Me); 0.4 (Me-Si). ^{29}Si NMR (99 MHz, $CDCl_3$, 298 K): δ −107.8. HRMS (EI): m/z calcd for $C_{57}H_{47}N_4O_5Si^+$: 895.3321, found: 895.3320 $[M+H]^+$. UV−vis (CH_2Cl_2, 298 K): λ_{max} (log ε) = 472 (6.09), 500 (5.87), 657 (5.46), 690 nm (5.19).

15. The careful titration of **8** at 230 K with solution of trifluoroacetic acid in dichloromethane-d_2 afforded the quantitative transformation of **8** into **15**. Initially the sample was cooled to 230 K. The solution of TFA was introduced into the sample through the microsyringe. The progress of the reaction was followed by ^{1}H NMR spectroscopy.

^{1}H NMR (500 MHz, CD_2Cl_2, 230 K): δ 7.52 (d, 2H, Tol); 7.51 (d, 1H, Tol); 7.47 (d, 1H, Pyrr); 7.46 (d, 1H, Tol); 7.42−7.36 (m, 9H, Tol); 7.38 (d, 1H, Pyrr); 7.34 (d, 1H, Pyrr.); 7.31 (d, 1H, Tol); 7.30 (d, 1H, Pyrr); 7.27 (d, 1H, Tol); 7.19 (d, 1H, Pyrr); 7.18 (d, 1H, Tol); 7.11 (d, 1H, Pyrr); 4.14, 3.83 (2d, 2H, $^2J_{(H,H)}$ = 24 Hz, 7, 7′); 2.49, 2.45, 2.43, 2.40 (4s, 12H, 5-*p*-Me, 10-*p*-Me, 15-*p*-Me, 20-*p*-Me); 0.98, 0.55 (2s, 6H, 9′-Me(1), 9′-Me(2)); −0.16 (s, 3H, Me-Si). ^{29}Si NMR (99 MHz, CD_2Cl_2, 230 K): δ −95.0.

Instrumentation. NMR spectra were recorded on Bruker Avance 500 and 600 MHz spectrometers. Absorption spectra were recorded on a Varian Cary 50 Bio spectrometer. Mass spectra were recorded on Bruker micrOTOF-Q and AD-604 spectrometers using the electrospray, liquid-matrix secondary ion mass spectrometry and electron impact techniques.

Computational Chemistry. DFT calculations were performed using Gaussian 03.[63] Geometry optimizations were carried out within unconstrained *C*1 symmetry, with starting coordinates pre-optimized using semiempirical methods. Becke′s three-parameter exchange functional[64] with the gradient-corrected correlation formula of Lee, Yang, and Parr (B3LYP)[65] was used with the 6-31G** basis set. The structures were found to have converged to a minimum on the potential energy surface; the resulting zero-point vibrational energies were included in the calculation of relative energies. Absolute ^{1}H shielding values were calculated at the GIAO-RHF/6-31G** level of theory using the B3LYP geometries. The chemical shift values were subsequently calculated relative to tetramethylsilane (TMS, absolute shielding: 31.75 ppm).

Acknowledgment. Financial support from the Ministry of Science and Higher Education (Grant PBZ-KBN-118/T09/2004) is kindly acknowledged. Quantum chemical calculations have been carried out at the Poznań Supercomputer Center (Poznań) and Wrocław Supercomputer Center (Wrocław).

Supporting Information Available: Tables of computational results (Cartesian coordinates); figures presenting correlations between calculated and experimental ^{1}H NMR chemical shifts; additional NMR data are included. This material is available free of charge via the Internet at http://pubs.acs.org.

(63) Frisch, M. J.; Trucks, G. W.; Schlegel, H. B.; Scuseria, G. E.; Robb, M. A.; Cheeseman, J. R.; Montgomery, J. A., Jr.; Vreven, T.; Kudin, K. N.; Burant, J. C.; Millam, J. M.; Iyengar, S. S.; Tomasi, J.; Barone, V.; Mennucci, B.; Cossi, M.; Scalmani, G.; Rega, N.; Petersson, G. A.; Nakatsuji, H.; Hada, M.; Ehara, M.; Toyota, K.; Fukuda, R.; Hasegawa, J.; Ishida, M.; Nakajima, T.; Honda, Y.; Kitao, O.; Nakai, H.; Klene, M.; Li, X.; Knox, J. E.; Hratchian, H. P.; Cross, J. B.; Adamo, C.; Jaramillo, J.; Gomperts, R.; Stratmann, R. E.; Yazyev, O.; Austin, A. J.; Cammi, R.; Pomelli, C.; Ochterski, J. W.; Ayala, P. Y.; Morokuma, K.; Voth, G. A.; Salvador, P.; Dannenberg, J. J.; Zakrzewski, V. G.; Dapprich, S.; Daniels, A. D.; Strain, M. C.; Farkas, O.; Malick, D. K.; Rabuck, A. D.; Raghavachari, K.; Foresman, J. B.; Ortiz, J. V.; Cui, Q.; Baboul, A. G.; Clifford, S.; Cioslowski, J.; Stefanov, B. B.; Liu, G.; Liashenko, A.; Piskorz, P.; Komaromi, I.; Martin, R. L.; Fox, D. J.; Keith, T.; Al-Laham, M. A.; Peng, C. Y.; Nanayakkara, A.; Challacombe, M.; Gill, P. M. W.; Johnson, B.; Chen, W.; Wong, M. W.; Gonzalez, C.; Pople, J. A. *Gaussian 03*, Revision C.01; Gaussian,Inc.: Pittsburgh, PA, 2004.

(64) Becke, A. D. *Phys. Rev. A* **1988**, *38*, 3098–3100.

(65) Lee, C.; Yang, W.; Parr, R. G. *Phys. Rev. B* **1988**, *37*, 785–789.